in the phosphorylation level of FAK or paxillin by the cortactin siRNAs in either HSC44PE cells or HSC57 cells (Fig. 2B).

To confirm the role of hyperphosphorylated cortactin in these cells, we also generated MCF7 cell lines that have elevated tyrosine phosphorylation of cortactin. Original MCF7 cells showed high expression of cortactin with the minimum level of tyrosine phosphorylation (Fig. 1A) and low expression of Fyn kinase (Fig. 2C). A vector expressing the Flag-tagged Fyn kinase was introduced into MCF7 cells, and several clones with stable expression of Fyn kinase were isolated, and two of these clones were named as MCF-Fyn1 and MCF-Fyn2. The amount of Fyn protein in both cells was ~10-fold greater than that of endogenous Fyn kinase in original MCF7 cells (Fig. 2C). Marked hyperphosphorylation of cortactin was observed in these two clones where Fyn kinase was introduced whereas original MCF7 cells or mock-transfected cells (MCF-Vec) were not (Fig. 2C). Knockout of cortactin greatly enhanced tyrosine phosphorylation of p130Cas both in MCF-Fyn1 cells and MCF-Fyn2 cells but not in MCF7-Vec cells (Fig. 2D and data not shown). These consistent results suggest that hyperphosphorylated cortactin may inhibit tyrosine phosphorylation of p130Cas in both HSC44PE and MCF-Fyn cells. Knockdown of cortactin also increased cell motility in both MCF-Fyn1 and MCF-Fyn2 cells whereas it blocked cell migration in parental MCF7 cells and MCF-Vec cells (Figs. 1C and 2E; data not shown). Similar results were obtained in the study using gastric cancer cells and it was shown that hyperphosphorylation of cortactin switches the response of cell motility.

Because many reports have shown the significant role of phosphorylation of p130Cas in cell migration, we examined whether knockdown of p130Cas by siRNA impairs the cell motility of HSC44PE cells treated or not treated with cortactin siRNA. Double treatment of Cas-siRNA and cort-siRNA completely impaired cell motility as well as treatment by Cas-siRNA alone, showing that p130Cas plays a dominant role in the regulation of cell motility of HSC44PE cells (Fig. 3B). These results indicate the possibility that hyperphosphorylated cortactin may suppress cell migration through inhibiting tyrosine phosphorylation of p130Cas.

Recruitment of p130Cas to Focal Adhesion by Treatment of Cortactin siRNA

To further investigate the cause of tyrosine phosphorylation of p130Cas induced by knockdown of cortactin, we analyzed the subcellular localization of p130Cas, cortactin, and focal adhesion proteins in HSC44PE cells. Total cortactin was widely expressed near the cell membrane in HSC44PE cells (Fig. 4A and B) whereas phosphorylated cortactin detected by a phosphospecific antibody against cortactin Y421 appeared at a specific domain, which seems to be focal adhesion within the cell membrane (Fig. 4B). It was further shown that phosphotyrosine-containing cortactin was clearly colocalized with vinculin, which is expressed at focal adhesion (Fig. 4C). By the treatment with cortactin siRNA, both the signals detected by total cortactin and cortactin Y421 were significantly weakened, suggesting these signals are cortactin specific (Fig. 4A).

In the control cells, p130Cas is mainly distributed in the cytoplasm and only slightly expressed at focal adhesion (Fig. 5B, *top*). When cortactin is knocked down, a substantial amount of p130Cas comes to locate at focal adhesion (Fig. 5B, *bottom*), suggesting the loss of cortactin-induced membrane localization of p130Cas. On the other hand, tyrosine-phosphorylated p130Cas detected by phosphospecific antibody was specifically localized at the focal adhesion although the amount of tyrosine phosphorylation was greatly increased by the suppression of cortactin expression (Fig. 5A). This observation may support the model that tyrosine-phosphorylated cortactin expressed predominantly in focal adhesions interferes with the localization of p130Cas at the focal adhesion, which causes tyrosine-phosphorylated p130Cas. Loss of hyperphosphorylated cortactin could therefore recruit p130Cas to the focal adhesion, which results in tyrosine phosphorylation of p130Cas, followed by enhancement of cell motility.

Discussion

We explored the role of cortactin in cell motility by using RNA interference technique in several gastric cancer cell lines that show various phosphorylation states of cortactin. It was

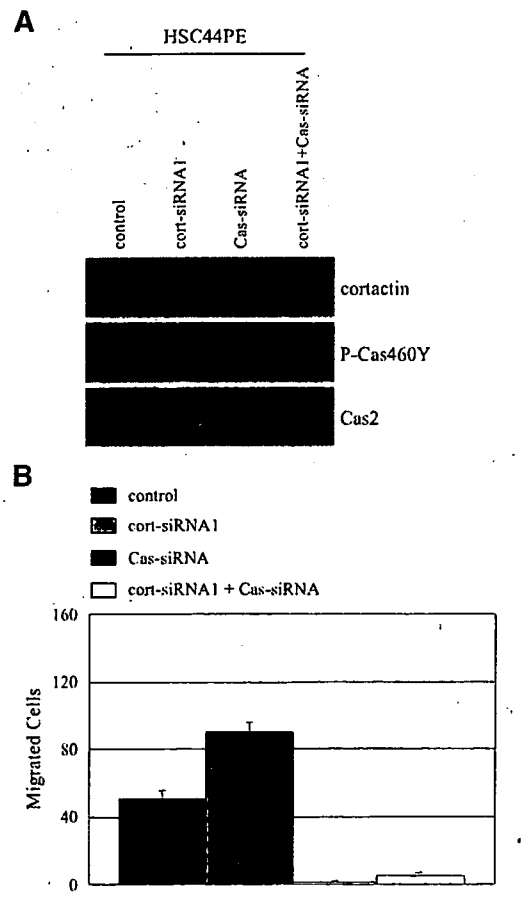

FIGURE 3. Knockdown of p130Cas blocks cell migration of HSC44PE cells regardless of the expression of cortactin. **A** and **B.** HSC44PE cells were treated with either cortactin siRNA or p130Cas siRNA alone, or both, and cell migration was analyzed as described. **A.** Expression of cortactin, p130Cas (Cas2), and phosphorylated p130Cas (pCas460Y) was analyzed to check the effect of each siRNA. **B.** By treatment with siRNA of Cas, cell migration of HSC44PE cells was totally inhibited regardless of the amount of cortactin expression.

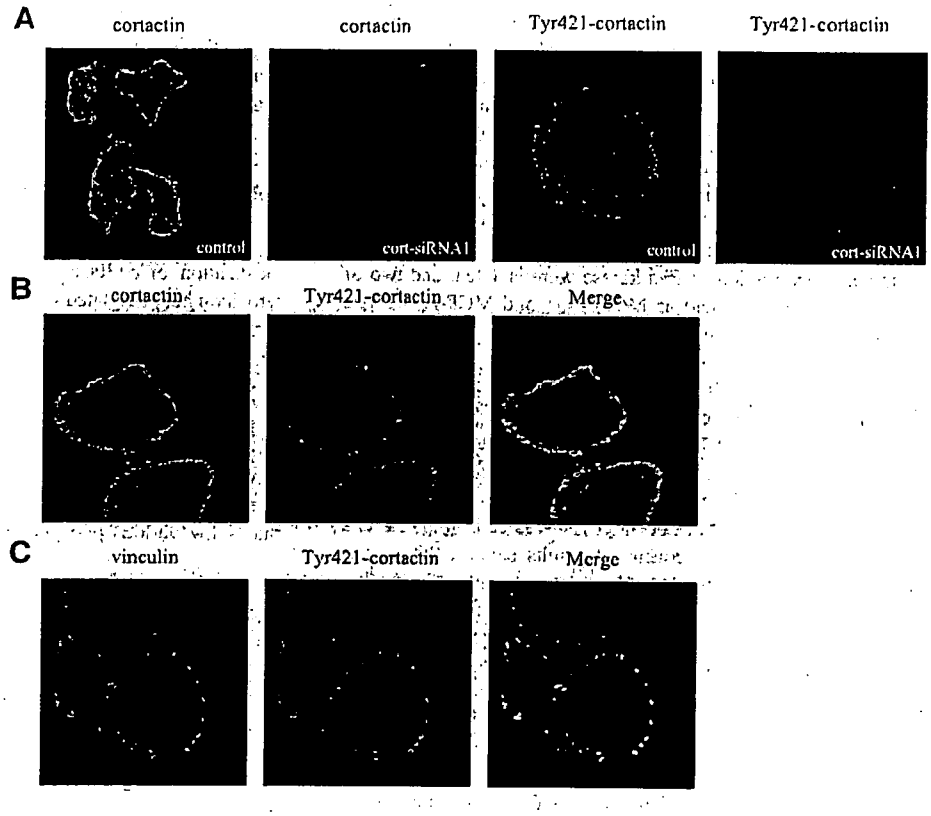

FIGURE 4. Localization of cortactin and tyrosine-phosphorylated cortactin in HSC44PE cells. **A.** HSC44PE cells were transfected with cortactin siRNA or control siRNA for 72 h followed by immunocytostaining with anti-cortactin (*green*) and anti-phospho-cortactin (Tyr^{421}: *red*) antibody. **B.** HSC44PE cells were immunostained with anti-phospho-cortactin (Tyr^{421}: *red*) and anti-cortactin (*green*) antibodies. **C.** HSC44PE cells were immunostained with anti-phospho-cortactin (Tyr^{421}: *red*) and anti-vinculin (*green*) antibodies. Merged image (*Merge*) indicates that tyrosine-phosphorylated cortactin localizes at focal adhesions that are stained by anti-vinculin.

revealed that knockdown of cortactin results in enhanced cell motility along with increased tyrosine phosphorylation of p130Cas in the cells that have hyperphosphorylated cortactin, whereas it impairs cell migration in the cells with a low level of tyrosine-phosphorylated cortactin. In addition, knockdown of hyperphosphorylated cortactin caused recruitment of p130Cas to focal adhesion, which might result in enhanced cell migration. In this study, for the first time, we showed that cortactin has a dual function in the regulation of cell motility, which depends on its tyrosine phosphorylation state.

Amplification and overexpression of the cortactin gene, *EMS1*, have been identified in various cancers (2, 3, 6, 23). In our previous study, overexpression and elevated tyrosine phosphorylation of cortactin was selectively observed in the metastatic subgroup of murine melanoma cells with high migratory potential (16). Based on these results, we first hypothesized that the hyperphosphorylated cortactin may promote cell migration in cancer cells. In this study, gastric cancer cells that have hyperphosphorylated cortactin showed at least similar or higher migration potential compared with those cells with basal levels of tyrosine phosphorylation of cortactin (Fig. 1A and C). However, unexpectedly, knockdown of cortactin in these cells further enhanced cell migration. The effect of cortactin knockdown was opposite in the cells with a low level of cortactin phosphorylation. This paradoxical outcome by cortactin knockdown was also confirmed in breast cancer cells MCF7, which expressed a significant amount of cortactin although the level of tyrosine phosphorylation was quite low. Introduction of Fyn kinase to MCF7 cells significantly enhanced the tyrosine phosphorylation of cortactin. In this condition, loss of cortactin by siRNA enhanced cell migration whereas it had a negative effect on cell migration in the parental cells. Based on this finding, cortactin hyperphosphorylation may be induced as a negative feedback mechanism when cells acquire highly migratory potential.

Some of the studies have shown that knockdown of cortactin results in impaired cell motility in hepatocellular carcinoma and head and neck squamous cell carcinoma cells (24, 25), whereas other studies have shown no significant effect on cell motility (8, 26), although all these studies lack information on the phosphorylation states of cortactin. Because it is suggested that cortactin differentially functions in cell migration depending on its phosphorylation state, the previous controversial results from the knockdown of cortactin should be reevaluated from the viewpoint of its tyrosine phosphorylation state. A previous study shows positive effect of the cortactin phosphorylation on the cell migration by overexpression of normal cortactin and phosphorylation-defective mutants in the endothelial cells (27). Although this study does not mention about the level of tyrosine phosphorylation of endogenous cortactin either, it might be weak in normal endothelial cells. Therefore, the positive effect of cortactin expression shown in the study might be consistent with our result using HSC57 or MCF7 cells, whereas the dominant-negative effect of phosphorylation-defective mutant might indicate some different function of cortactin in the endothelial cells.

In our observation, knockdown of cortactin induced outstanding enhancement in tyrosine phosphorylation of

p130Cas. Because there is no significant change in the phosphorylation of other substrates of SFKs such as FAK and paxillin, it is indicated that there exists some specific mechanism underlying the regulation of tyrosine phosphorylation state of p130Cas by cortactin. Unphosphorylated p130Cas is mainly expressed in the cytoplasm as shown in Fig. 5B, whereas localization of p130Cas in the focal adhesion is thought to be required for tyrosine phosphorylation of p130Cas (28, 29). The results of immunocytostaining indicate that tyrosine-phosphorylated cortactin predominantly exists in the focal adhesion, and thus purging p130Cas from focal adhesion to lose the chance of being phosphorylated. Therefore, knockdown of cortactin might give chance for p130Cas to localize at the focal adhesion to be phosphorylated (Fig. 5). p130Cas was originally found as a prominent substrate of SFKs, including c-Src and Fyn during the transformation of cells (21, 30). It has been shown that phosphorylated p130Cas in focal adhesion plays a regulatory role in cell spreading and cell migration (19, 31-33), and knockdown of p130Cas actually abrogated cell migration in our gastric cancer cells, HSC44PE, even in the absence of cortactin (Fig. 3A and B). These results indicate that activation of p130Cas-mediated signal might be responsible for the enhancement of cell motility in the cells where hyperphosphorylated cortactin is knocked down.

Our study sheds new light on the cross-talk between cortactin and p130Cas, both of which are Src substrates. Such cross-regulation between SFK substrates might give more optimized outcome out of overlapping or conflicting effects of SFK signals. However, there is still a possibility that phosphorylated cortactin may also transduce specific signals regulating cell migration, which is independent of a function of p130Cas. As far as we examined, there was no significant effect on the morphology, cell-matrix adhesion, or number of focal adhesions in HSC44PE cells by suppression of cortactin expression (Fig. 5A and data not shown). On the other hand, it has been suggested that cortactins originally support cell migration through several pathways and therefore its tyrosine phosphorylation may have an inhibitory effect on these pathways. Binding of cortactin with N-WASP via its SH3 domain may synergize in causing actin polymerization

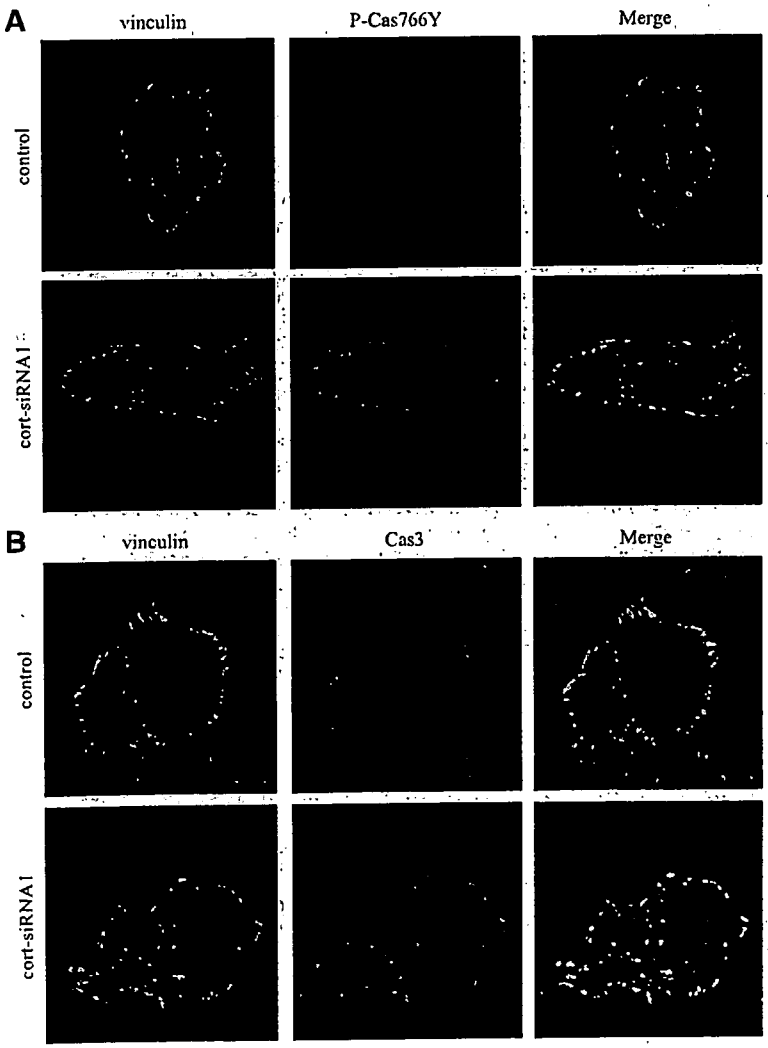

FIGURE 5. Changes in localization of p130Cas by treatment with cortactin siRNA. **A.** HSC44PE cells were transfected with cortactin siRNA or control siRNA for 72 h, before localization of phosphorylated p130Cas was analyzed by immunocytostaining with P-Cas766Y antibody. Anti-vinculin antibody was used to visualize focal adhesions. Merged images indicate that tyrosine-phosphorylated p130Cas, which was greatly increased by cortactin siRNA, specifically localizes at focal adhesion. **B.** In HSC44PE cells treated with control or cortactin siRNA, localization of p130Cas was analyzed by anti-Cas3 antibody. A portion of p130Cas shows distinct colocalization with vinculin at focal adhesion in cells treated with cortactin siRNA, whereas staining of vinculin and p130Cas did not significantly overlapped in cells treated with control siRNA.

preceding cell migration, which is promoted by a serine kinase Erk and conversely inhibited by Src kinase (34). We showed all these signal pathways of phosphorylated cortactin in a schema (Fig. 6). In summary, tyrosine phosphorylation of cortactin might act as a unique and naïve switch in the regulation of cell motility. Our study offers new insight into cortactin for understanding its biological function in cancer progression.

Materials and Methods

Cell Culture

Human breast cancer cell line MCF7 was maintained in DMEM containing 10% (v/v) fetal bovine serum (Life Technologies) and 50 μg/mL penicillin-streptomycin antibiotics. Human gastric cancer cell lines HSC57, HSC44As3, HSC44PE, and HSC58As9 was supplied by Central Animal Laboratory, National Cancer Center Institute, Tokyo, Japan (24). They were maintained in RPMI 1640 supplemented with 10% fetal bovine serum and antibiotics.

Antibodies and Reagents

Anti-phosphotyrosine (4G10) and anti-cortactin (clone 4F11) antibodies were obtained from Upstate Biotechnology. Polyclonal antibodies Fyn3 and anti-FAK were purchased from Santa Cruz Biotechnology. Anti-paxillin and anti-green fluorescent protein (GFP) antibodies were purchased from Zymed and MBL, respectively. Anti-phospho-paxillin (Tyr^{118}), anti-phospho-FAK (Tyr^{397}), and anti-phospho-cortactin (Tyr^{421}) antibodies were purchased from Cell Signaling Technology, Upstate Biotechnology, and Chemicon, respectively. Anti-Flag-M2 antibody was obtained from Sigma. Polyclonal antibodies against p130Cas (Cas2 and Cas3) and phosphospecific polyclonal antibody P-Cas460Y were used as described previously (30, 35). Another phosphospecific antibody, P-Cas766Y, was generated by immunizing rabbits with a synthetic phosphopeptide, CMEDpYDpYVHL, which includes the phosphotyrosine-containing motifs in the Src-binding domain of p130Cas, after being conjugated with thymoglobulin. As secondary antibodies, horseradish peroxidase-conjugated anti-rabbit and anti-mouse IgG (Amersham) were used. Polylysine, fibronectin, and cycloheximide were purchased from Sigma. Inhibitor of SFKs, 4-amino-5-(4-chlorophenyl)-7-(*t*-butyl) pyrazolo [3,4-*d*] pyrimidine (PP2), and the inactive structural analogue 4-amino-7-phenylpyrazol [3,4-*d*] pyrimidine (PP3) were obtained from Calbiochem-Novabiochem Ltd.

RNA Interference Experiments for Cortactin and p130Cas

Two independent siRNA of human cortactin, cort-siRNA1 and cort-siRNA2, for RNA interference experiment were generated by Invitrogen Life Technologies. Cort-siRNA1 targets cortactin mRNA at 5′-CCCAGAAAGACUAUGUGAAAGG-GUU-3′ and Cort-siRNA2 targets at 5′-GGAGAAGCACGA-GUCACAGAGAGAU-3′. The siRNA of human p130Cas was also generated by Invitrogen Life Technologies, using the target sequence 5′-CCAAGAUCUUUGUGGCGCACAGCAA-3′. For transient transfection of siRNA, the cells were plated at 1.5×10^5 per well on a six-well plate. Transfection of siRNAs was done with Lipofectamine 2000 (Invitrogen Co.). After transfection for 72 h, the cells were harvested for the biochemical analyses.

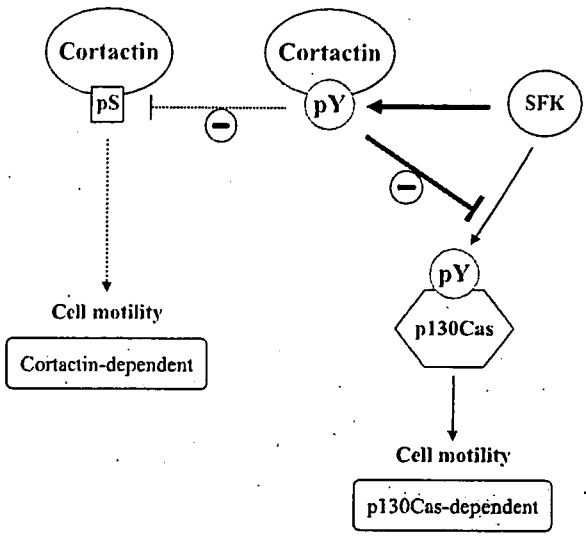

FIGURE 6. Schematic view of multiple roles of cortactin in the regulation of cancer cell motility.

Infection of Retroviral Constructs

Retrovirus vectors were used to express mouse cortactin fused with GFP (pJl6) and F421F466F482 triple mutant of mouse cortactin fused with GFP (pJL12; ref. 4). Briefly, the retroviral vector and the packaging construct pCL-10A1 were cotransfected into 293T cells and culture fluid was harvested 72 h posttransfection. HSC44PE cells were infected with the viral fluid in the presence of 4 mg/mL polybrene, and the infected cells were selected in the presence of 800 μg/mL Geneticin G418 (Sigma) for a period of 2 to 3 wk.

Establishment of Stable MCF7 Clones Expressing Fyn Kinase

Breast cancer cells MCF7 were grown in DMEM containing 10% fetal bovine serum and antibiotics. On the night before transfection, the cells were seeded onto a 10-cm dish at a density of 9.0×10^5. Transfection of a vector expressing Fyn kinase with a tag of Flag (Fyn-Flag) and an original vector (pcDNA3.1) was done according to the manufacturer's instructions. Twenty-four hours after transfection, the cells were subjected to selection by Geneticin G418 (Sigma) at a concentration of 800 μg/mL for a period of 2 to 3 wk.

Immunoblotting and Immunoprecipitation

For immunochemical analysis, cells were cultured in the incubator at 37°C with 5% CO_2 for 48 to 72 h, before the cells were lysed in 1% Triton X-100 buffer (50 mmol/L HEPES, 150 mmol/L NaCl, 10% glycerol, 1% Triton X-100, 1.5 mmol/L $MgCl_2$, 1 mmol/L EGTA, 100 mmol/L NaF, 1 mmol/L Na_3VO_4, 10 μg/mL aprotinin, 10 μg/mL leupeptin, 1 mmol/L phenylmethylsulfonyl fluoride), and insoluble material was removed by centrifugation for 10 min. Protein concentration was analyzed by BCA Protein Assay (Pierce), and the protein

aliquots were separated by SDS-PAGE. Gels were transferred to the polyvinylidene difluoride membrane (Millipore) and subjected to immunoblotting. After blocking with 5% skim milk in TBST [100 mmol/L Tris-HCl (pH 8.0), 150 mmol/L NaCl, and 0.05% Tween 20] for 1 h, blots were incubated with primary antibodies. In the case of 4G10, blocking was done with Blocking One Solution (Nakarai Co.). Membranes were then washed thrice with TBST, incubated with horseradish peroxidase–conjugated secondary antibodies for 30 min at room temperature, washed thrice by TBST again and once by TBS [100 mmol/L Tris-HCl (pH 8.0), 150 mmol/L NaCl], and visualized by autoradiography using a chemiluminescence reagent (Western Lighting, Perkin-Elmer).

For immunoprecipitation, 500 μg of protein were mixed with 2 μg of antibodies and incubated for 1 h on ice, and then samples were rotated with protein G–Sepharose beads (Amersham Pharmacia) for 2 h at 4°C. The beads were washed thrice with 1% Triton X-100 buffer and boiled in sample buffer [2% SDS, 0.1 mol/L Tris-HCl (pH 6.8), 10% glycerol, 0.01% bromphenol blue, 0.1M DTT] for SDS-PAGE analysis.

Immunocytostaining

Approximately 5×10^4 cells were plated on 12-mm circle cover glasses on a 24-well plate, which were grown in DMEM with 10% fetal bovine serum at 37°C with 5% CO_2 for 24 h. The 12-mm circle cover glasses were coated by fibronectin 10 μg/mL in PBS overnight before seeding the cells. Then, cells were fixed in 4% paraformaldehyde in 0.1 mol/L sodium phosphate (pH 7.0) for 5 min, washed thrice with PBS, and permeabilized with 0.1% Triton X-PBS for 10 min before blocking with 5% bovine serum albumin with TBST [0.15 mol/L NaCl, 1% Tris (pH 7.0), 0.05% Tween 20] for 10 min. Then, the cells were incubated with the first antibody for 1 h at room temperature. Cells were washed with PBS thrice, and incubated with appropriate second Alexa antibodies (Molecular Probe; 1:500) in 5% goat serum with 3% bovine serum albumin/TBST. All cover glasses were mounted in 1.25% DABCO, 50% PBS, and 50% glycerol. The staining was visualized using a Radiance 2100 confocal microscopic system (Bio-Rad).

Cell Migration Assay

Migration assay was done using modified Transwell chambers with polycarbonate Nucleopore membrane (Falcon, BD). Precoated filters (6.5 mm in diameter, 8-μm pore size, fibronectin 10 μg/mL) were rehydrated with 100 μL medium. Then, 4×10^4 cells in 100 μL serum-free DMEM supplement were seeded onto the upper part of each chamber, whereas the lower compartments were filled with 600 μL of the same medium with 10% fetal bovine serum. Following incubation for 8 h at 37°C, nonmigrated cells on the upper surface of the filter were wiped out with a cotton swab, and the migrated cells on the lower surface of the filter were fixed and stained with Giemsa stain solution (Azur-Eosin-Methylene Blue Solution, Muto Pure Chemicals, Co., Japan). The total number of migrated cells was determined by counting cells in five microscopic fields per well at a magnification of ×100, and the extent of migration was expressed as the average number of the cells per microscopic field.

Acknowledgments

We thank Dr. Xi Zhan for mouse cortactin constructs and Dr. Hitoyasu Futami for critical reading of the manuscript.

References

1. Schuuring E, Verhoeven E, Litvinov S, Michalides RJ. The product of the EMS1 gene, amplified and overexpressed in human carcinoma, is homologous to a v-src substrate and is located in cell-substratum contact sites. Mol Cell Biol 1993;13:2891–8.

2. Campbell DH, deFazio A, Sutherland RL, Daly RJ. Expression and tyrosine phosphorylation of EMS1 in human breast cancer cell line. Int J Cancer 1996;68: 485–92.

3. Hui R, Ball JR, Macmillan RD, et al. EMS1 gene expression in primary breast cancer relationship to cyclin D1 and oestrogen receptor expression and patient survival. Oncogene 1998;17:1053–9.

4. Li Y, Tondravi M, Liu J, et al. Cortactin potentates bone metastasis of breast cancer cells. Cancer Res 2001;61:6906–11.

5. Patel AM, Incognito LS, Schechter GL, Wasilenko WJ, Somers KD. Amplification and expression of EMS-1 (cortactin) in head and neck squamous cell carcinoma cell lines. Oncogene 1996;12:31–5.

6. Freier K, Sticht C, Hofele C, et al. Recurrent coamplification of cytoskeleton-associated genes EMS1 and SHANK2 with CCND1 in oral squamous cell carcinoma. Genes Chromosomes Cancer 2006;45:118–25.

7. Daly RJ. Cortactin signaling and dynamic actin networks. Biochem J 2004; 382:13–25.

8. Lua BL, Low BC. BPGAP1 interacts with cortactin and facilitates its translocation to cell periphery for enhanced cell migration. Mol Biol Cell 2004; 15:2873–83.

9. Du Y, Weed SA, Xiong WC, Marshall TD, Parsons JT. Identification of a novel cortactin SH3 domain-binding protein and its localization to growth cones of cultured neurons. Mol Cell Biol 1998;18:5838–51.

10. Kowalski JR, Egile C, Gil S, Snapper SB, Li R, Thomas SM. Cortactin regulates cell migration through activation of N-WASP. J Cell Sci 2005;118: 79–87.

11. Wu H, Parsons JT. Cortactin, an 80/85-kilodalton pp60src substrate, is a filamentous actin-binding protein enriched in the cell cortex. J Cell Biol 1993; 120:1417–26.

12. Kim L, Wong TW. Growth factor-dependent phosphorylation of the actin-binding protein cortactin is mediated by the cytoplasmic tyrosine kinase FER. J Biol Chem 1998;273:23542–8.

13. Gallet C, Rosa JP, Habib A, Lebret M, Levy-Toledano S Maclouf J. Tyrosine phosphorylation of cortactin associated with Syk accompanies thromoxane analogue-induced platelet shape change. J Biol Chem 1999;274: 23610–6.

14. Campbell DH, Sutherland RL, Daly RJ. Signaling pathways and structural domains required for phosphorylation of EMS1/cortactin. Cancer Res 1999;59: 5376–85.

15. Vidal CB, Geny J, Melle M, Jandrot-Perrus M, Fontenay-Roupie. Cdc42/ Rac1-dependent activation of the p21-activated kinase (PAK) regulates human platelet lamellipodia spreading implication of the cortical-actin binding protein cortactin. Blood 2002;100:4462–9.

16. Huang J, Asawa T, Takato T Sakai R. Cooperative roles of Fyn and cortactin in cell migration of metastatic murine melanoma. J Biol Chem 2003; 278:48367–76.

17. Webb DJ, Parsons JT, Horwitz AF. Adhesion assembly, disassembly and turnover in migrating cells—over and over and over again. Nat Cell Biol 2002;4: 97–100.

18. Mitchison TJ, Cramer LP. Actin-base cell motility and cell locomotion. Cell 1996;84:371–9.

19. Honda H, Oda H, Nakamoto T, et al. Cardiovascular anomaly, impaired actin bundling and resistance to Src-induced transformation in mice lacking p130Cas. Nat Genet 1998;19:361–5.

20. Huang J, Hamasaki H, Nakamoto T, et al. Differential regulation of cell migration, actin stress fiber organization, and cell transformation by functional domains of Crk-associated substrate. J Biol Chem 2002;277:27265–72.

21. Sakai R, Nakamoto T, Ozawa K, Aizawa S, Hirai H. Characterization of the kinase activity essential for tyrosine phosphorylation of p130Cas in fibroblasts. Oncogene 1997;14:1419–26.

22. Yanagihara K, Tanaka H, Takigahira M, et al. Establishment of two cell lines from human gastric scirrhous carcinoma that possess the potential to metastasize spontaneously in nude mice. Cancer Sci 2004;95:575–82.

23. Zhang LH, Tian B, Diao LR, et al. Dominant expression of 85-kDa form of cortactin in colorectal cancer. J Cancer Res Clin Oncol 2006;132:113–20.

24. Chuma M, Sakamoto M, Yasuda J, et al. Overexpression of cortactin is involved in motility and metastasis of hepatocellular carcinoma. J Hepatol 2004; 41:629–36.

25. Rothschild BL, Shim AH, Ammer AG, et al. Cortactin overexpression regulates actin-related protein 2/3 complex activity, motility, and invasion in carcinomas with chromosome 11q13 amplification. Cancer Res 2006;66: 8017–25.

26. Barroso C, Rodenbusch SE, Welch MD, Drubin DG. A role for cortactin in *Listeria monocytogenes* invasion of NIH 3T3 cells, but not in its intracellular motility. Cell Motil Cytoskeleton 2006;63:231–43.

27. Nakamoto T, Sakai R, Honda H, et al. Requirements for localization of p130cas to focal adhesions. Mol Cell Biol 1997;17:3884–97.

28. Huang C, Liu J, Haudenschild CC, Zhan X. The role of tyrosine phosphorylation of cortactin in the locomotion of endothelial cells. J Biol Chem 1998;273:25770–6.

29. Sawada Y, Tamada M, Dubin-Thaler BJ, et al. Force sensing by mechanical extension of the Src family kinase substrate p130Cas. Cell 2006; 127:1015–26.

30. Sakai R, Iwamatsu A, Hirano N, et al. A novel signaling molecule, p130, forms stable complexes *in vivo* with v-Crk and v-Src in a tyrosine phosphorylation-dependent manner. EMBO J 1994;13:3748–56.

31. Klemke RL, Leng J, Molander R, Brooks PC, Vuori K, Cheresh DA. CAS/Crk coupling servers as a "molecular switch" for induction of cell migration. J Cell Biol 1998;140:961–72.

32. Panetti TS. Tyrosine phosphorylation of paxillin, FAK and p130CAS: effects on cell spreading and migration. Front Biosci 2002;7:143–50.

33. Pratt SJ, Epple H, Ward M, Feng Y, Braga VM, Longmore GD. The LIM protein Ajuba influences p130Cas localization and Rac1 activity during cell migration. J Cell Biol 2005;168:813–24.

34. Martinez-Quiles N, Ho HY, Kirschner MW, Ramesh N, Geha RS. Erk/Src phosphorylation of cortactin acts as a switch on-switch off mechanism that controls its ability to activate N-WASP. Mol Cell Biol 2004;24:5269–80.

35. Miyake I, Hakomori Y, Misu Y, et al. Domain-specific function of ShcC docking protein in neuroblastoma cells. Oncogene 2005;24:3206–15.

Possible Role of Semaphorin 3F, a Candidate Tumor Suppressor Gene at 3p21.3, in p53-Regulated Tumor Angiogenesis Suppression

Manabu Futamura, Hiroki Kamino, Yuji Miyamoto, Noriaki Kitamura, Yasuyuki Nakamura, Shiho Ohnishi, Yoshiko Masuda, and Hirofumi Arakawa

Cancer Medicine and Biophysics Division, National Cancer Center Research Institute, Tsukiji, Chuo-ku, Tokyo, Japan

Abstract

Although the regulation of tumor angiogenesis is believed to be one of the core functions of p53, the mechanism still remains to be elucidated. Here, we report that semaphorin 3F (*SEMA3F*), an axon guidance molecule, is involved in p53-regulated antiangiogenesis. The expression level of *SEMA3F* mRNA was increased by both exogenous and endogenous p53. Chromatin immunoprecipitation assay indicated that a potent p53-binding sequence in intron 1 of *SEMA3F* interacts with p53 and that it has a p53-responsive transcriptional activity. Overexpression of *SEMA3F* inhibited *in vitro* cell growth of the lung cancer cell line H1299. In nude mice assay, the size of the H1299 tumors expressing SEMA3F was much smaller, and they showed lesser number of blood vessels as compared with the control tumors. Moreover, tumors derived from the p53-knockdown colorectal cancer cell line LS174T displayed a remarkable enhancement of tumor vessel formation as compared with control tumors containing normal levels of p53. The expression levels of *SEMA3F* and neuropilin-2 (*NRP2*), the functional receptor for SEMA3F, in p53-knockdown LS174T tumors were lower than those in the control tumors. Adenovirus-mediated *SEMA3F* gene transfer induced the remarkable *in vitro* growth suppression of the stable transformant of H1299 cells, which express high levels of NRP2. These results suggest that p53 negatively regulates tumor vessel formation and cell growth via the SEMA3F-NRP2 pathway. [Cancer Res 2007;67(4):1451–60]

Introduction

The tumor suppressor p53 prevents malignant transformation when the cells suffer cellular stresses including severe DNA damage (1). Hence, p53 is known as a "guardian of human genome" (2). Indeed, *p53* is mutated in >50% of all human cancers, emphasizing its essential role in tumorigenesis in any of the human cancers. Because of its importance, numerous studies on p53 have been conducted thus far, and several findings have been reported. These efforts have provided concrete evidence for the following functions of p53. The *p53* gene encodes a transcription factor that binds to a specific sequence of its downstream target gene (3). Therefore, p53 exerts its functions via transcriptional activation of various target genes (3, 4). Although a considerable number of target genes have been reported, their functions display great diversity, and four major ones, including genes functioning in cell cycle arrest, apoptosis, DNA repair, and antiangiogenesis, are considered to be involved in the core mechanism of p53-regulated tumor suppression (1, 3, 4).

Because angiogenesis plays a critical role in tumor formation and progression, blocking tumor angiogenesis is one of vital antitumor functions. An inhibitor of angiogenesis was previously detected in the condition medium derived from glioblastoma cells, wherein exogenous p53 was overexpressed (5). This implies that p53 may activate the transcription of an antiangiogenic factor gene. Consistent with this assumption, thrombospondin-1 (TSP-1), which is a pivotal factor for angiogenesis, was identified as the transcriptional target gene of p53 by using cultured fibroblast cells from Li-Fraumeni patients (6). This fact confirmed that p53 might play an important role in the control of angiogenesis during tumor development. In addition, a study reported that brain-specific angiogenesis inhibitor 1 (BAI1) is the second example of p53-regulated antiangiogenic factor (7). Although these two molecules are really interesting and promising candidates, the precise mechanism of p53-regulated antiangiogenesis still remains to be elucidated.

Semaphorins are a highly conserved family of molecules that contribute to axon guidance during neural development and differentiation by repulsing axons and inhibiting growth cone extension (8–11). Based on their structure, they are classified into seven subclasses, including transmembrane proteins (classes 1, 4, 5, and 6), secreted proteins (classes 2 and 3), and proteins associated with the cell surface through glycosylphosphatidylinositol linkages (class 7; ref. 12). Semaphorin 3F (SEMA3F) belongs to the class 3 secreted type of semaphorin protein (12). During the developmental process, SEMA3F plays a critical role in axon guidance in both the peripheral nervous system and the central nervous system by interacting with its receptor, neuropilin-2 (NRP2; ref. 13). The SEMA3F-NRP2 signaling pathway guides axonal extension by means of a chemotactic repulsing effect on the axons (14–16).

Although semaphorins play a critical role as axon guidance molecules in the developing nervous system, they are expressed in a variety of adult and embryonic tissues, suggesting a broader spectrum of the functions for semaphorins. In fact, *SEMA3F* was initially identified as a candidate tumor suppressor gene at chromosome 3p21.3; loss of heterozygosity from 3p21.3 is frequently observed in many cases of human cancers (17–19). In particular, the region is most frequently deleted and at least one allele is lost in nearly 100% of the cases of small-cell lung cancer (20, 21). Although extensive analysis was conducted, no point mutations in *SEMA3F* were detected in human cancers (17–19).

Note: Supplementary data for this article are available at Cancer Research Online (http://cancerres.aacrjournals.org/).

Requests for reprints: Hirofumi Arakawa, Cancer Medicine and Biophysics Division, National Cancer Center Research Institute, 5-1-1 Tsukiji, Chuo-ku, Tokyo 104-0045, Japan. Phone: 81-3-3547-5273; Fax: 81-3-3546-1369; E-mail: harakawa@gan2.res.ncc.go.jp.

doi:10.1158/0008-5472.CAN-06-2485

Instead, the expression of *SEMA3F* was frequently down-regulated epigenetically in a number of cancers, implying that alterations of *SEMA3F* may be involved in tumorigenesis (22). Moreover, overexpression of *SEMA3F* in cancer cells induced the growth suppression of some cancer cells (23). Despite these observations, the role of SEMA3F in tumorigenesis remains controversial.

Here, we report yet another finding that implies that *SEMA3F* is a bona fide tumor suppressor gene. In the present study, we have found that *SEMA3F* is a direct target gene for tumor suppressor p53 and that SEMA3F is likely to mediate p53-regulated antiangiogenesis during tumor development. Additionally, it is likely that NRP2 expression is also controlled by p53. Our findings suggest a novel p53-regulated mechanism of antiangiogenesis and cell growth suppression via the SEMA3F-NRP2 pathway.

Materials and Methods

Cell culture. Human cancer cell lines HepG2 (hepatoblastoma), H1299 (lung cancer), T98G (Glioblastoma), LS174T (colon cancer), and MCF7 (breast cancer) were purchased from the American Type Culture Collection (Manassas, VA). Colon cancer cell lines HCT116 p53(+/+) and HCT116 p53(−/−) were a gift from Dr. Bert Vogelstein (Johns Hopkins University, Baltimore, MD). All cells were cultured under the conditions recommended by their respective depositors.

RNA interference. By using two cancer cell lines (HepG2 and LS174T) containing wild-type p53 (wt-p53), we established p53-knockdown cell lines (HepG2-p53-siRNA and LS174T-p53-siRNA) and control cell lines (HepG2-control and LS174T-control) as previously described (24). In brief, these cells were infected with SI-MSCV-puro-H1R-p53Ri retrovirus for down-regulation of p53 expression and with SI-MSCV-puro-H1R retrovirus for negative control. Then, the infected cells were selected with 1 μg/mL puromycin for 2 weeks and the single clones were isolated.

Northern blot analysis. Northern blot analysis was done as previously described (25). HepG2 cells were infected with adenovirus p53 (Ad-p53) or adenovirus green fluorescent protein (Ad-EGFP) at 30 multiplicity of infection (MOI), or two kinds of the p53-knockdown, and the control cell lines were treated with 1 μg/mL Adriamycin (doxorubicin) for 2 h. mRNAs were isolated from the cells collected at the indicated times. Probes carrying the coding sequences of *SEMA3F*, *p21/WAF1*, and *β-actin* were labeled with [α-^{32}P]dCTP using Megaprime DNA labeling system (GE Healthcare Bio-Sciences, Piscataway, NJ). The blots were hybridized with the radioactive probes at 42°C for 16 h, washed, exposed to Phosphor Screen, and visualized with Storm 860 (Molecular Dynamics, Sunnyvale, CA).

Western blot. Western blot analysis was carried out as previously described (26). After treatment of each cell line with 1 μg/mL Adriamycin, total cell lysates were prepared in radioimmunoprecipitation assay buffer [150 mmol/L NaCl, 50 mmol/L Tris-HCl (pH 8.0), 0.1% SDS, 1% NP40, protease inhibitor cocktail]. Anti-p53 (Ab-6; Calbiochem, San Diego, CA), anti-β-actin antibody (AC-74; Sigma, St. Louis, MO), polyclonal anti-NRP2 antibody (C9; Santa Cruz Biotechnology, Santa Cruz, CA), and anti-FLAG (M2) monoclonal antibody (Sigma) were used in Western blot analysis.

Chromatin immunoprecipitation assay. Chromatin immunoprecipitation assays were done using the chromatin immunoprecipitation assay kit from Upstate Biotechnology (Lake Placid, NY) as recommended by the manufacturer and as previously described (26). The anti-p53 monoclonal antibody (Ab12; Calbiochem) for immunoprecipitation and the anti-FLAG M2 monoclonal antibody (Sigma) as a negative control were used. H1299 (1.5×10^6) or HepG2 (1.5×10^6) cells were plated onto 10-cm dish and infected with Ad-p53 or Ad-EGFP at 30 MOI. HCT116 p53(+/+) and HCT116 p53(−/−) cells (3×10^6) were treated with 1 μg/mL Adriamycin to activate endogenous p53. The PCRs were done with the following specific primers: SEMA3F-p53BS1, 5′-AGTATCGAAGCTCTCTGAGG-3′ and 5′-CCTGATAA-CAGCTGTGGATAT-3′; SEMA3F-p53BS2, 5′-GGGGAGAAAGGAGAAAGCAT-3′ and 5′-GTTCTTTGGCCTGCCTTTGT; NRP2-p53BS1, 5′-TCTGGCATAGT-CATGCATCC-3′ and 5′-CTGAGACCTTTAGCATGTTCAAACTA; NRP2-p53BS2, 5′-GTTCACGGCCGATGCTTCA-3′ and 5′-TGAGCGTGGATCTCC-TATCT; and p21, 5′-ACCTTTCACCATTCCCCTAC-3′ and 5′-GCCCAAGGA-CAAAATAGCCA-3′.

Luciferase assay. The 172-bp fragment including p53BS1 and the 193-bp fragment of p53BS2, which were amplified with the same primers as in the chromatin immunoprecipitation assays, were cloned into pGL3 promoter vector (Promega, Madison, WI) and sequenced. For NRP2, the 249-bp fragment including p53BS1 was cloned into pGL3 promoter vector. Reporter assay was done as previously described (26). p53 family genes, such as *p73* and *p63*, and four expression constructs (pRc/CMV-p73α, pRc/CMV-p73β, pRc/CMV-p63α, and pRc/CMV-p63γ; refs. 27, 28) were a gift from Shuntaro Ikawa (Tohoku University, Sendai, Japan). pGL3 vector with p53BS for p21 was used for positive control.

Plasmid construction. The entire coding region of *SEMA3F* amplified by reverse transcription-PCR (RT-PCR) was cloned into pCR-Blunt II-TOPO vector (Invitrogen, Carlsbad, CA) and sequenced. The fragment containing the whole *SEMA3F* sequence was digested with *Eco*RI and cloned into pcDNA3.1(+) (Invitrogen) to prepare sense-strand SEMA3F (pcDNA-SEMA3F-S) and antisense-strand SEMA3F (pcDNA-SEMA3F-AS) for colony formation assay, or into pIRES-EGFP (BD Biosciences, San Jose, CA) for stable transformants expressing the EGFP signal that represents the expression level of *SEMA3F* mRNA. The entire *SEMA3F* cDNA with *Eco*RI and *Xba*I sites was amplified by PCR, sequenced, and then cloned into p3×FLAG-CMV-14 expression vector (Sigma), which contains three tandems of FLAG peptides at the COOH terminus for generating Ad-FLAG-SEMA3F. For NRP2-expressing vector, the cDNA clone containing the entire coding region of *NRP2* was purchased from RZPD German Resource Center for Genome Research (Berlin, Germany). The entire coding region of NRP2, amplified by PCR, was also cloned into pCR-Blunt II-TOPO vector and sequenced. The fragment containing the whole *NRP2* sequence was digested with *Xba*I and *Hin*dIII and cloned into pcDNA3.1(−) for stable transformants.

Construction of recombinant adenoviruses for SEMA3F. Replication-deficient recombinant viruses Ad-SEMA3F and Ad-3×FLAG-SEMA3F were generated and purified as previously described (29). In brief, blunt-ended SEMA3F and 3×FLAG-tagged SEMA3F containing 3×FLAG at a COOH terminus of SEMA3F were cloned into the *Sml*I site of the cosmid pAxCAwtit (Takara, Otsu, Japan), which contains the CAG promoter and the entire genome of type 5 adenovirus except for E1 and E3 regions. BspT104I-digested cosmids were transfected to 293 (human embryonic kidney cell line) cells. Viruses were propagated in 293 cells and purified as previously described. Expression levels of SEMA3F-expressing adenoviruses were evaluated by Western blot for Ad-3×FLAG-SEMA3F or by RT-PCR for Ad-SEMA3F at 24 h postinfection at the indicated MOIs.

Cell viability assay. To examine the role of the SEMA3F-NRP2 pathway in cell growth, we examined cell viability using trypan blue exclusion method. Parental H1299 cells and the NRP2-stable transformant cells (s-11; 1.5×10^5) were plated onto six-well culture plates and infected with either Ad-SEMA3F or Ad-3×FLAG-SEMA3F at 0, 5, 10, 30, 60, and 100 MOIs. Ad-EGFP was used as a negative control. Seventy-two hours later, all the cell components were collected and viable cells were counted by hemocytometer.

Nude mice assay. Nude mice assay was done by inoculating the SEMA3F stable transformants and LS174T-p53-si cells. For SEMA3F stable transformants, two independent clones (I-s11 and I-s17) and a control cell line (IRES1) were inoculated s.c. into the bilateral thoracic and abdominal walls (total four parts per mouse) of 7w-female BALB/c AJcl-nu mice (CLEA Japan, Tokyo, Japan) at 1×10^6 per mouse in a volume of 0.1 mL. LS174T-p53-si and LS174T-control cells were also inoculated at 2×10^6 per mouse. Then the mice were maintained under specific pathogen-free conditions. The tumor volume was measured with a caliper twice a week and assessed by the formula (width × width × length) / 2. After 2 to 5 weeks of observation, explanted tumors were isolated and analyzed genetically and immunohistochemically. These animal experiments were repeated twice to confirm the similar results. These animal experimental protocols were approved by the Committee for Ethics of Animal Experimentation and the experiments were conducted in accordance with the Guidelines for Animal Experiments in the National Cancer Center.

Semiquantitative RT-PCR. The excised tumors were homogenized and total RNAs were extracted by TRIzol. cDNAs were synthesized from 3 μg of total RNA with SuperScript First-Strand Synthesis System (Invitrogen). The RT-PCR was run in the exponential region (19–30 cycles) to allow semiquantitative comparisons among cDNAs developed from identical reactions. Each PCR regimen involved a 94°C, 5 min initial denaturation step followed by 19 cycles (*β2-MG*), 21 cycles (*SEMA3F, BAI1*, and *VEGF*), 22 cycles (*p53* and *p21/WAF1*), 24 cycles (*TSP1*), 25 cycles (*NRP1*), 30 cycles (*NRP2*), 55°C for 30 s, and 72°C for 30 s on a GeneAmp PCR system 9700 (Applied Biosystems, Foster City, CA).

Immunohistochemistry. The frozen sections (6 μm) from the resected tumors embedded into optimum cutting temperature (OCT) compound (Sakura Fine Technical, Tokyo, Japan) were stained by immunoperoxidase procedure. Briefly, after air dry, each section was fixed with cold acetone, treated with 0.3% H_2O_2 for 10 min, and then blocked with 10% goat serum. Antimouse CD31 (MEC13.3; BD Biosciences) was used as the first antibody (1:100) and incubated at room temperature for 1 h. Then Histofine Simplestain MAX-PO (rat; Nichirei, Tokyo, Japan) was incubated at room temperature for 30 min as the second antibody and visualized with 3-amino-9-ethylcarbazole substrate (Nichirei). The consecutive sections corresponding to mCD31 staining sections were used for H&E staining. Light images of immunofluorescent tissues were viewed under an Olympus IX71 microscope (Olympus, Tokyo, Japan) and digitized using Olympus DP70 camera and DP70-BSW software (Olympus).

Tumor vessel density. For analysis of vessel density, 8 to 10 independent tumors were randomly selected from each group (I-s11, I-s17, IRES1, LS174T-p53-siRNA, and LS174T-control). CD31-positive areas showing tumor vessels were captured using NIH Image software. In each section, vascular-rich fields with the maximum proportion of vessel density in each field were compared. Vessel densities were calculated as the ratio of the CD31-positive area divided by the total area (30, 31).

Statistical analysis. Colony numbers in colony formation assay, tumor volume, tumor weight, and tumor vessel density in nude mice assay were analyzed by Student's *t* test.

Results

Identification of *SEMA3F* as a novel p53-inducible gene. The emerging evidence suggested the role of axon guidance molecules in tumorigenesis (4, 32). In addition, semaphorin 3B (*SEMA3B*) was previously reported to be regulated by tumor suppressor p53 (33). Therefore, we reasoned that SEMA3F may be involved in the p53-regulated transcriptional network. To test this hypothesis, we first carried out Northern blot analysis of the *SEMA3F* gene. mRNAs were subjected to Northern blot analysis, which were obtained at the indicated time after infection from the HepG2 cells, a hepatocellular carcinoma cell line, infected with adenovirus p53 (Ad-p53) or adenovirus EGFP (Ad-EGFP). As shown in Fig. 1*A*, a 3.8-kb transcript of *SEMA3F* was detected, and the expression was increased in the cells infected with Ad-p53, whereas the increase was very small in the Ad-EGFP-infected cells, suggesting that exogenous p53 can induce the expression of *SEMA3F*. Clear induction was also observed in the case of the *p21/WAF1* gene, one of the most well-known p53-inducible genes (Fig. 1*A*).

To further validate the p53 dependency of the *SEMA3F* expression, we examined whether endogenous p53 activates the transcription of *SEMA3F*. We established p53-knockdown cell lines derived from HepG2 cells and LS174T cells (a colorectal cancer cell line). As indicated in Fig. 1*B*, the expression of endogenous p53 protein was increased after treatment with 1 μg doxorubicin in HepG2-control and LS174T-control cells, whereas negligible p53 expression was detected in HepG2-p53-siRNA and LS174T-p53-siRNA cells. Similarly, the expression of *SEMA3F* mRNA was induced in both the control cells, but its expression was not increased in both the p53-siRNA cells (Fig. 1*C*). These results, when considered together, indicated that the transcription of

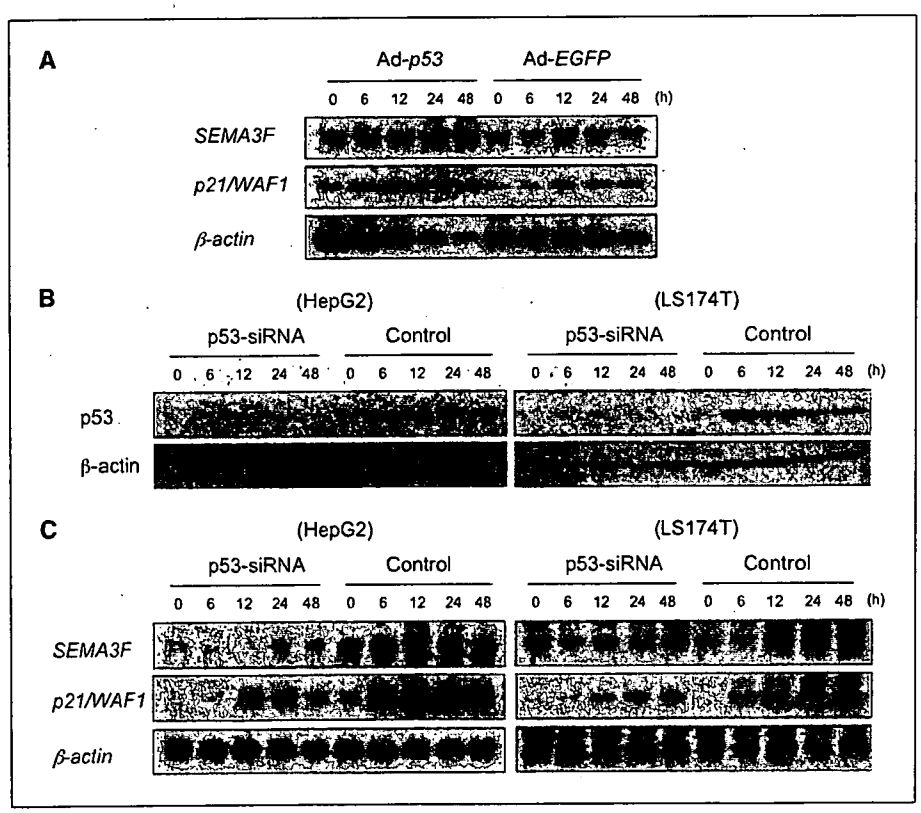

Figure 1. *SEMA3F* as a p53-inducible gene. *A*, exogenous p53-dependent expression of *SEMA3F*. mRNAs isolated at the indicated times from the HepG2 cells infected with Ad-p53 or Ad-EGFP at an MOI of 30 were subjected to Northern blot analysis for the *SEMA3F* gene. *p21/WAF1* and *β-actin* were used as positive and loading controls, respectively. *B*, expression of p53 protein. The cell lysates isolated at the indicated times from p53-siRNA and control cells, which were derived from either HepG2 cells or LS174T cells, were subjected to Western blot analysis for p53. *β-actin* was used as a loading control. *C*, endogenous p53–dependent expression of *SEMA3F*. mRNAs isolated at the indicated times from p53-siRNA and control cells (HepG2 or LS174T), which were treated with 0.2 μg/mL Adriamycin, were subjected to Northern blot analysis for the *SEMA3F* gene. *p21/WAF1* and *β-actin* were used as positive and loading controls, respectively.

SEMA3F is activated by endogenous and exogenous p53 and that *SEMA3F* is a novel p53-inducible gene.

***SEMA3F* as a direct transcriptional target of p53.** To determine whether *SEMA3F* is a direct target gene of p53, we investigated p53-binding sequence(s) (p53BS) in the genomic region and found two candidate sequences, BS1 and BS2, in intron 1 of *SEMA3F* (Fig. 2*A*). Therefore, we did a chromatin immunoprecipitation assay. The protein complex, including p53 and the chromatin-associated DNA fragments, was immunoprecipitated with the anti-p53 antibody and the precipitated DNA was subjected to PCR analysis with the specific primers for BS1 and BS2. As shown in Fig. 2*B*, the sequence of BS1, but not BS2, was clearly amplified by PCR with the protein complex immunoprecipitated from H1299 cells infected with Ad-p53 or from HCT116-p53(+/+) cells treated with 0.2 μg doxorubicin, implying that both exogenous and endogenous p53 interact with BS1.

To determine whether BS1 actually has p53-dependent transcriptional activity, we carried out a reporter assay. A 200- to 300-bp DNA fragment containing BS1 or BS2 was cloned upstream of the SV40 promoter of pGL3-promoter vector (pGL3-BS1 or pGL3-BS2). As indicated in Fig. 2*C*, when pGL3-BS1 was cotransfected with wild-type p53-plasmid, but not mutant p53-plasmid, the luciferase activity was remarkably enhanced. In addition, it is noted that p73β also activated the transcription of pGL3-BS1 (Fig. 2*D*). These results suggest that *SEMA3F* is a bona fide target gene of p53 and possibly p73β.

The role of SEMA3F in cell growth. To examine the role of SEMA3F in *in vitro* cell growth, we first did colony formation assay. As shown in Supplementary Fig. S1*A* and *B*, overexpression of sense *SEMA3F* caused significant reduction in the H1299 cell colony number as compared with overexpression of antisense *SEMA3F*, whereas no significant difference was observed between sense *SEMA3F*– and antisense *SEMA3F*–transfected T98G cells. The difference in the results between H1299 and T98G is likely to be due to the expression level of NRP2, which is a functional receptor for SEMA3F, because the expression level of *NRP2* in H1299 was higher than that of T98G (data not shown).

Although significant growth suppression by SEMA3F was observed, the effect seemed to be mild. Therefore, we attempted to establish stable H1299 cell transformants, which consistently express high levels of SEMA3F. The sense sequence of *SEMA3F* was cloned into the pIRES2-EGFP vector, which has the internal ribosomal site of the encephalomyocarditis virus, between the multiple cloning site and the *EGFP* gene to be translated from a single bicistronic mRNA. Therefore, it is possible to monitor the expression level of *SEMA3F* by examining the EGFP signal. Eventually, we selected two independent clones, pIRES-SEMA3F-11 (l-s11) and pIRES-SEMA3F-17 (l-s17). As indicated in Supplementary Fig. S2*A*, homogeneous and high levels of green signals of EGFP were detected in these two clones. Consistent with the result of EGFP, the high expression of *SEMA3F* mRNA was also detected by RT-PCR (Supplementary Fig. S2*B*). As seen in Supplementary Fig. S1*A*, the high and stable expression of SEMA3F inhibited the *in vitro* cell growth to some extent, but the effect was not dramatic (Supplementary Fig. S2*C*).

The role of SEMA3F in tumor growth. To investigate the role of SEMA3F in tumor growth, three types of the established cell lines, including control, pIRES-SEMA3F-11 (l-s11), and pIRES-SEMA3F-17 (l-s17), were s.c. implanted on the flank of nude mice. Then, the tumor volume of each tumor was measured

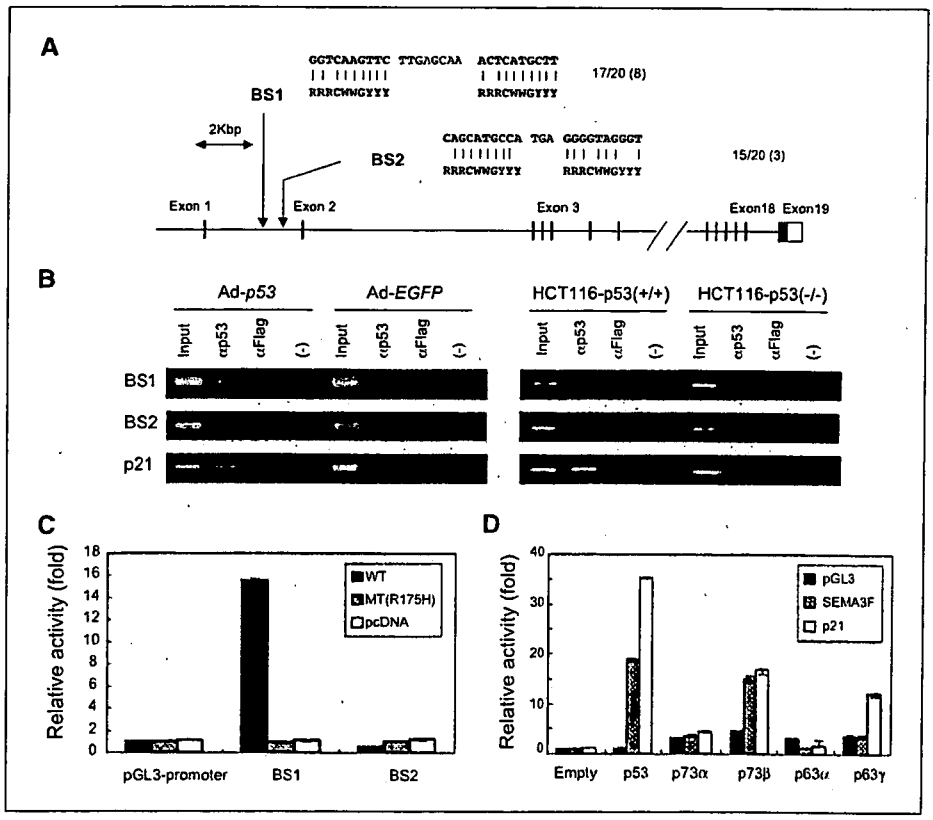

Figure 2. Identification of *SEMA3F* as a direct target gene of p53. *A*, potential p53-binding sequences. Two potential p53-binding sequences, BS1 and BS2, are located in intron 1 of *SEMA3F*. *B*, binding of p53 with BS1 of *SEMA3F*. Chromatin immunoprecipitation assay was done for the DNA-protein complex, which was immunoprecipitated by anti-p53 antibody from H1299 cells infected with Ad-p53 or Ad-EGFP at an MOI of 30, or from HCT116-p53(+/+) cells or HCT116-p53(−/−) cells treated with 0.2 μg/mL Adriamycin. *p21/WAF1* was used as a positive control. *C*, p53-dependent transcriptional activity of BS1. The heterologous luciferase reporter plasmid containing BS1 or BS2 was cotransfected with the plasmid designed to express wild-type p53 (*p53WT*), mutant p53 (*p53MT*), or no p53 (mock) into H1299 cells. The luciferase activity 24 h after transfection is shown in relation to the activity of the pGL3-promoter vectors without p53BSs. *D*, p73β-dependent transcriptional activity of BS1. The heterologous luciferase reporter plasmid containing BS1 was cotransfected with the plasmid designed to express wild-type p53 (p53), p73α, p73β, p63α, p63γ, or no p53 (mock) into H1299 cells. The luciferase activity 24 h after transfection is shown in relation to the activity of the pGL3-promoter vectors without p53BSs.

Semiquantitative RT-PCR. The excised tumors were homogenized and total RNAs were extracted by TRIzol. cDNAs were synthesized from 3 μg of total RNA with SuperScript First-Strand Synthesis System (Invitrogen). The RT-PCR was run in the exponential region (19–30 cycles) to allow semiquantitative comparisons among cDNAs developed from identical reactions. Each PCR regimen involved a 94°C, 5 min initial denaturation step followed by 19 cycles (*β2-MG*), 21 cycles (*SEMA3F, BAI1*, and *VEGF*), 22 cycles (*p53* and *p21/WAF1*), 24 cycles (*TSP1*), 25 cycles (*NRP1*), 30 cycles (*NRP2*), 55°C for 30 s, and 72°C for 30 s on a GeneAmp PCR system 9700 (Applied Biosystems, Foster City, CA).

Immunohistochemistry. The frozen sections (6 μm) from the resected tumors embedded into optimum cutting temperature (OCT) compound (Sakura Fine Technical, Tokyo, Japan) were stained by immunoperoxidase procedure. Briefly, after air dry, each section was fixed with cold acetone, treated with 0.3% H_2O_2 for 10 min, and then blocked with 10% goat serum. Antimouse CD31 (MEC13.3; BD Biosciences) was used as the first antibody (1:100) and incubated at room temperature for 1 h. Then Histofine Simplestain MAX-PO (rat; Nichirei, Tokyo, Japan) was incubated at room temperature for 30 min as the second antibody and visualized with 3-amino-9-ethylcarbazole substrate (Nichirei). The consecutive sections corresponding to mCD31 staining sections were used for H&E staining. Light images of immunofluorescent tissues were viewed under an Olympus IX71 microscope (Olympus, Tokyo, Japan) and digitized using Olympus DP70 camera and DP70-BSW software (Olympus).

Tumor vessel density. For analysis of vessel density, 8 to 10 independent tumors were randomly selected from each group (1-s11, 1-s17, IRES1, LS174T-p53-siRNA, and LS174T-control). CD31-positive areas showing tumor vessels were captured using NIH Image software. In each section, vascular-rich fields with the maximum proportion of vessel density in each field were compared. Vessel densities were calculated as the ratio of the CD31-positive area divided by the total area (30, 31).

Statistical analysis. Colony numbers in colony formation assay, tumor volume, tumor weight, and tumor vessel density in nude mice assay were analyzed by Student's *t* test.

Results

Identification of *SEMA3F* as a novel p53-inducible gene. The emerging evidence suggested the role of axon guidance molecules in tumorigenesis (4, 32). In addition, semaphorin 3B (*SEMA3B*) was previously reported to be regulated by tumor suppressor p53 (33). Therefore, we reasoned that SEMA3F may be involved in the p53-regulated transcriptional network. To test this hypothesis, we first carried out Northern blot analysis of the *SEMA3F* gene. mRNAs were subjected to Northern blot analysis, which were obtained at the indicated time after infection from the HepG2 cells, a hepatocellular carcinoma cell line, infected with adenovirus p53 (Ad-p53) or adenovirus EGFP (Ad-EGFP). As shown in Fig. 1*A*, a 3.8-kb transcript of *SEMA3F* was detected, and the expression was increased in the cells infected with Ad-p53, whereas the increase was very small in the Ad-EGFP-infected cells, suggesting that exogenous p53 can induce the expression of *SEMA3F*. Clear induction was also observed in the case of the *p21/WAF1* gene, one of the most well-known p53-inducible genes (Fig. 1*A*).

To further validate the p53 dependency of the *SEMA3F* expression, we examined whether endogenous p53 activates the transcription of *SEMA3F*. We established p53-knockdown cell lines derived from HepG2 cells and LS174T cells (a colorectal cancer cell line). As indicated in Fig. 1*B*, the expression of endogenous p53 protein was increased after treatment with 1 μg doxorubicin in HepG2-control and LS174T-control cells, whereas negligible p53 expression was detected in HepG2-p53-siRNA and LS174T-p53-siRNA cells. Similarly, the expression of *SEMA3F* mRNA was induced in both the control cells, but its expression was not increased in both the p53-siRNA cells (Fig. 1*C*). These results, when considered together, indicated that the transcription of

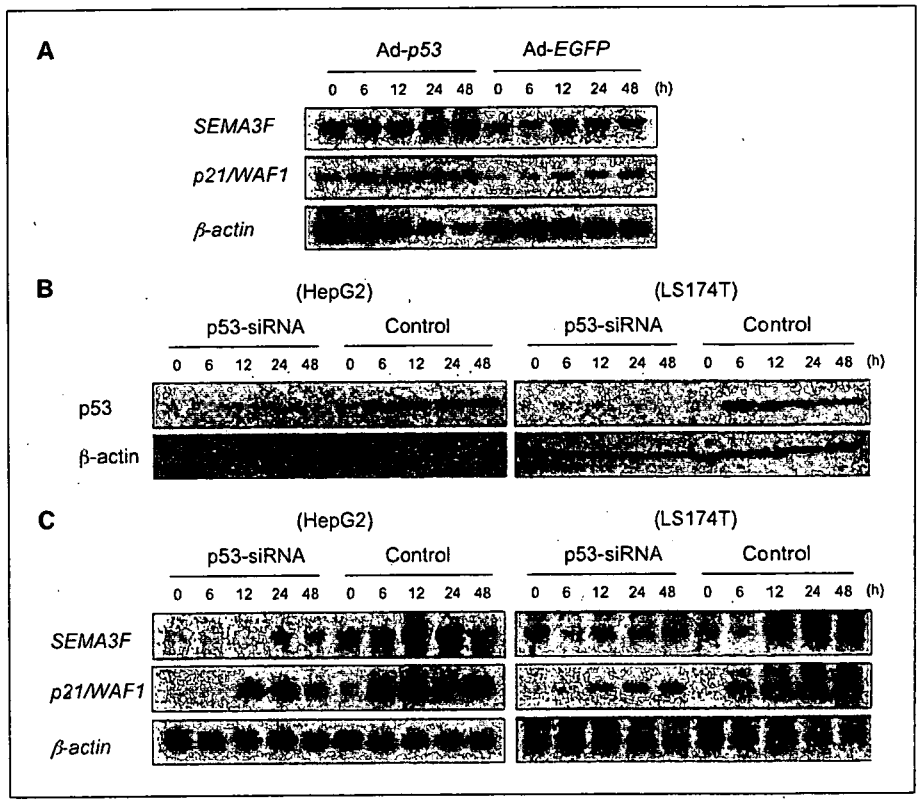

Figure 1. *SEMA3F* as a p53-inducible gene. *A*, exogenous p53-dependent expression of *SEMA3F*. mRNAs isolated at the indicated times from the HepG2 cells infected with Ad-p53 or Ad-EGFP at an MOI of 30 were subjected to Northern blot analysis for the *SEMA3F* gene. *p21/WAF1* and *β-actin* were used as positive and loading controls, respectively. *B*, expression of p53 protein. The cell lysates isolated at the indicated times from p53-siRNA and control cells, which were derived from either HepG2 cells or LS174T cells, were subjected to Western blot analysis for p53. *β-actin* was used as a loading control. *C*, endogenous p53–dependent expression of *SEMA3F*. mRNAs isolated at the indicated times from p53-siRNA and control cells (HepG2 or LS174T), which were treated with 0.2 μg/mL Adriamycin, were subjected to Northern blot analysis for the *SEMA3F* gene. *p21/WAF1* and *β-actin* were used as positive and loading controls, respectively.

SEMA3F is activated by endogenous and exogenous p53 and that *SEMA3F* is a novel p53-inducible gene.

***SEMA3F* as a direct transcriptional target of p53.** To determine whether *SEMA3F* is a direct target gene of p53, we investigated p53-binding sequence(s) (p53BS) in the genomic region and found two candidate sequences, BS1 and BS2, in intron 1 of *SEMA3F* (Fig. 2*A*). Therefore, we did a chromatin immunoprecipitation assay. The protein complex, including p53 and the chromatin-associated DNA fragments, was immunoprecipitated with the anti-p53 antibody and the precipitated DNA was subjected to PCR analysis with the specific primers for BS1 and BS2. As shown in Fig. 2*B*, the sequence of BS1, but not BS2, was clearly amplified by PCR with the protein complex immunoprecipitated from H1299 cells infected with Ad-p53 or from HCT116-p53(+/+) cells treated with 0.2 μg doxorubicin, implying that both exogenous and endogenous p53 interact with BS1.

To determine whether BS1 actually has p53-dependent transcriptional activity, we carried out a reporter assay. A 200- to 300-bp DNA fragment containing BS1 or BS2 was cloned upstream of the SV40 promoter of pGL3-promoter vector (pGL3-BS1 or pGL3-BS2). As indicated in Fig. 2*C*, when pGL3-BS1 was cotransfected with wild-type p53-plasmid, but not mutant p53-plasmid, the luciferase activity was remarkably enhanced. In addition, it is noted that p73β also activated the transcription of pGL3-BS1 (Fig. 2*D*). These results suggest that *SEMA3F* is a bona fide target gene of p53 and possibly p73β.

The role of SEMA3F in cell growth. To examine the role of SEMA3F in *in vitro* cell growth, we first did colony formation assay. As shown in Supplementary Fig. S1*A* and *B*, overexpression of sense *SEMA3F* caused significant reduction in the H1299 cell colony number as compared with overexpression of antisense *SEMA3F*, whereas no significant difference was observed between sense *SEMA3F*– and antisense *SEMA3F*–transfected T98G cells. The difference in the results between H1299 and T98G is likely to be due to the expression level of NRP2, which is a functional receptor for SEMA3F, because the expression level of *NRP2* in H1299 was higher than that of T98G (data not shown).

Although significant growth suppression by SEMA3F was observed, the effect seemed to be mild. Therefore, we attempted to establish stable H1299 cell transformants, which consistently express high levels of SEMA3F. The sense sequence of *SEMA3F* was cloned into the pIRES2-EGFP vector, which has the internal ribosomal site of the encephalomyocarditis virus, between the multiple cloning site and the *EGFP* gene to be translated from a single bicistronic mRNA. Therefore, it is possible to monitor the expression level of *SEMA3F* by examining the EGFP signal. Eventually, we selected two independent clones, pIRES-SEMA3F-11 (I-s11) and pIRES-SEMA3F-17 (I-s17). As indicated in Supplementary Fig. S2*A*, homogeneous and high levels of green signals of EGFP were detected in these two clones. Consistent with the result of EGFP, the high expression of *SEMA3F* mRNA was also detected by RT-PCR (Supplementary Fig. S2*B*). As seen in Supplementary Fig. S1*A*, the high and stable expression of SEMA3F inhibited the *in vitro* cell growth to some extent, but the effect was not dramatic (Supplementary Fig. S2*C*).

The role of SEMA3F in tumor growth. To investigate the role of SEMA3F in tumor growth, three types of the established cell lines, including control, pIRES-SEMA3F-11 (I-s11), and pIRES-SEMA3F-17 (I-s17), were s.c. implanted on the flank of nude mice. Then, the tumor volume of each tumor was measured

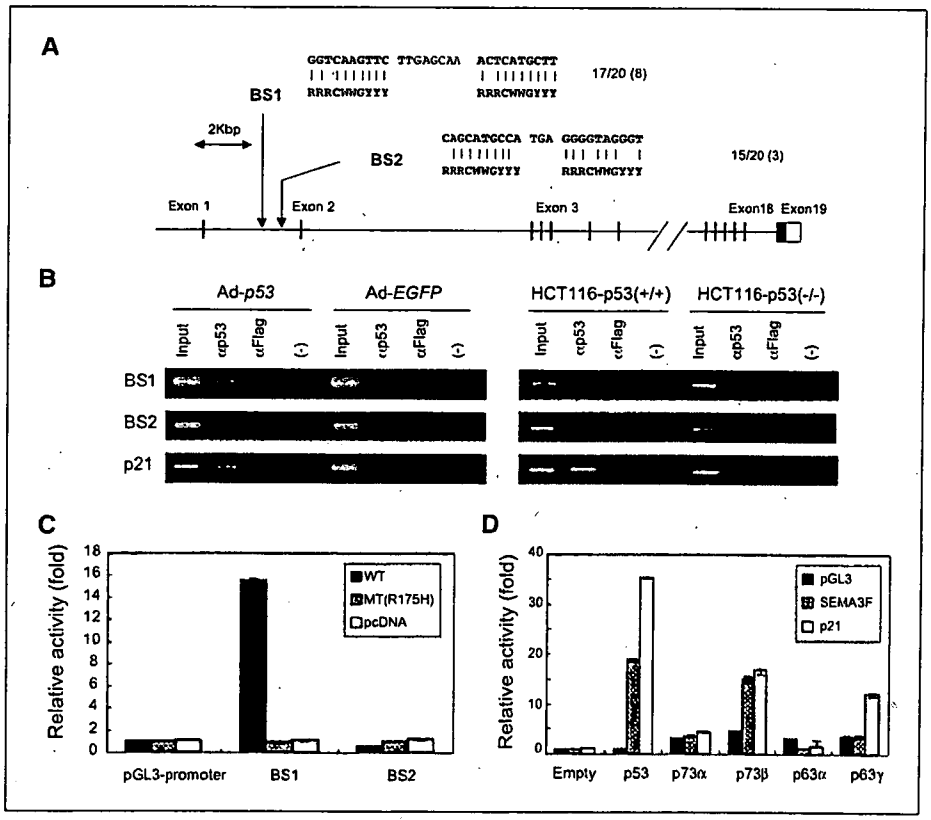

Figure 2. Identification of *SEMA3F* as a direct target gene of p53. *A*, potential p53-binding sequences. Two potential p53-binding sequences, BS1 and BS2, are located in intron 1 of *SEMA3F*. *B*, binding of p53 with BS1 of *SEMA3F*. Chromatin immunoprecipitation assay was done for the DNA-protein complex, which was immunoprecipitated by anti-p53 antibody from H1299 cells infected with Ad-p53 or Ad-EGFP at an MOI of 30, or from HCT116-p53(+/+) cells or HCT116-p53(−/−) cells treated with 0.2 μg/mL Adriamycin. *p21/WAF1* was used as a positive control. *C*, p53-dependent transcriptional activity of BS1. The heterologous luciferase reporter plasmid containing BS1 or BS2 was cotransfected with the plasmid designed to express wild-type p53 (*p53WT*), mutant p53 (*p53MT*), or no p53 (mock) into H1299 cells. The luciferase activity 24 h after transfection is shown in relation to the activity of the pGL3-promoter vectors without p53BSs. *D*, p73β-dependent transcriptional activity of BS1. The heterologous luciferase reporter plasmid containing BS1 was cotransfected with the plasmid designed to express wild-type p53 (p53), p73α, p73β, p63α, p63γ, or no p53 (mock) into H1299 cells. The luciferase activity 24 h after transfection is shown in relation to the activity of the pGL3-promoter vectors without p53BSs.

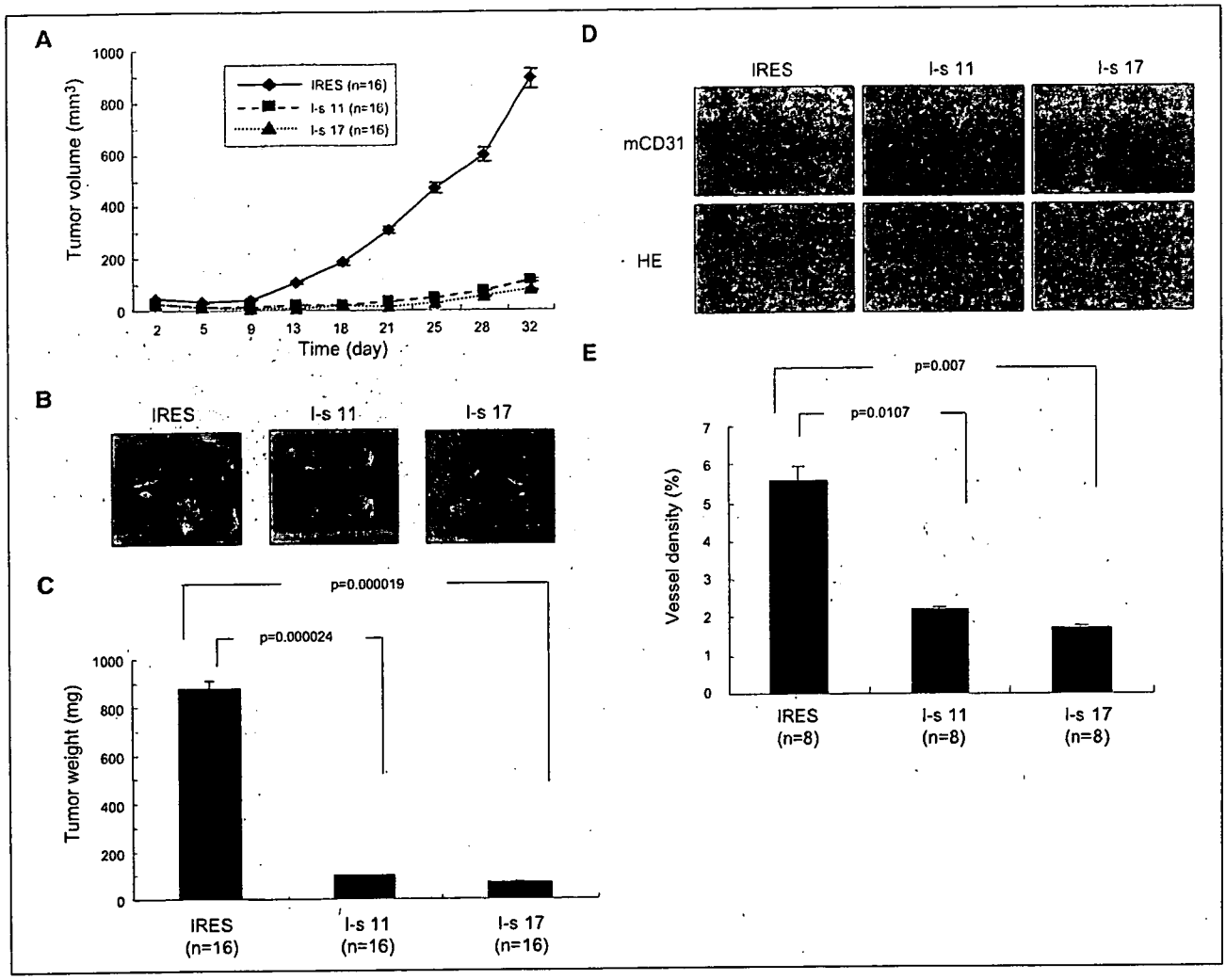

Figure 3. *In vivo* tumor growth suppression by SEMA3F. *A*, tumor volume. The tumor volume of each tumor derived from pIRES-control (IRES1), pIRES2-SEMA3F-11 (I-s 11), or pIRES-SEMA3F-17 (I-s 17) stable clone was measured twice every week following the establishment of xenografts in BALB/c AJcl-nu nude mice. *Bars*, SE. *B*, macroscopic appearance. The tumors were isolated at day 32 from each group. *C*, tumor weight. *Columns*, average tumor weight for each group; *bars*, SE. $P < 0.01$ was deemed statistically significant. *D*, immunohistochemistry for CD31 expression. Frozen sections of the isolated tumors were subjected to immunohistochemical staining with anti-CD31 antibody and H&E staining. Representative result from each group (×200). *E*, measurement of the area of tumor blood vessels. The area of tumor blood vessels stained with anti-CD31 antibody was measured in the intratumoral region. *Columns*, average area of tumor vessels for each group; *bars*, SE. $P < 0.01$ was deemed statistically significant.

twice a week for 32 days. As clearly indicated in Fig. 3*A*, the tumors derived from the control cell line grew exponentially, whereas the growth of the tumors from two independent SEMA3F-expressing clones was severely impaired. Moreover, the tumors derived from pIRES-SEMA3F-11 (I-s11) and pIRES-SEMA3F-17 (I-s17) cell lines were clearly much smaller in size and weight than those derived from the control cell line (Fig. 3*B* and *C*). The comparison between the results of Supplementary Figs. S1 and S2 and those of Fig. 3 indicated that the *in vivo* effect of SEMA3F on tumor growth was much stronger than the *in vitro* effect on cell growth, implying that SEMA3F might play an additional role *in vivo*.

The antiangiogenic role of SEMA3F in tumor growth suppression. SEMA3F was previously reported to play a role in developmental and tumor-associated angiogenesis (34–38). Therefore, we postulated that the remarkable effect on the *in vivo* tumor growth might be related to the regulation of tumor angiogenesis. Frozen sections from the tumors embedded in OCT compound were stained with mCD31, which is a specific vascular marker. As indicated in Fig. 3*D*, the number of tumor vessels in control tumors was much more than that in SEMA3F-expressing tumors (Fig. 3*E*). Moreover, the quantitative analysis of the area of tumor vessels in the intratumoral region clearly indicated that the area of tumor vessels in the control tumors was significantly larger as compared with that in the SEMA3F-expressing tumors (Fig. 3*E*). These results suggest that SEMA3F inhibits tumor angiogenesis, resulting in tumor growth suppression.

p53 negatively regulates tumor angiogenesis probably via the SEMA3F-NRP2 pathway. Although p53 has been suggested to play an important role in the inhibition of tumor angiogenesis, there exists little evidence to support this assumption. Therefore, we evaluated whether p53 is actually involved in the regulation of tumor angiogenesis. LS174T-control and LS174T-p53-siRNA cells were s.c. inoculated on the flank of nude mice and allowed

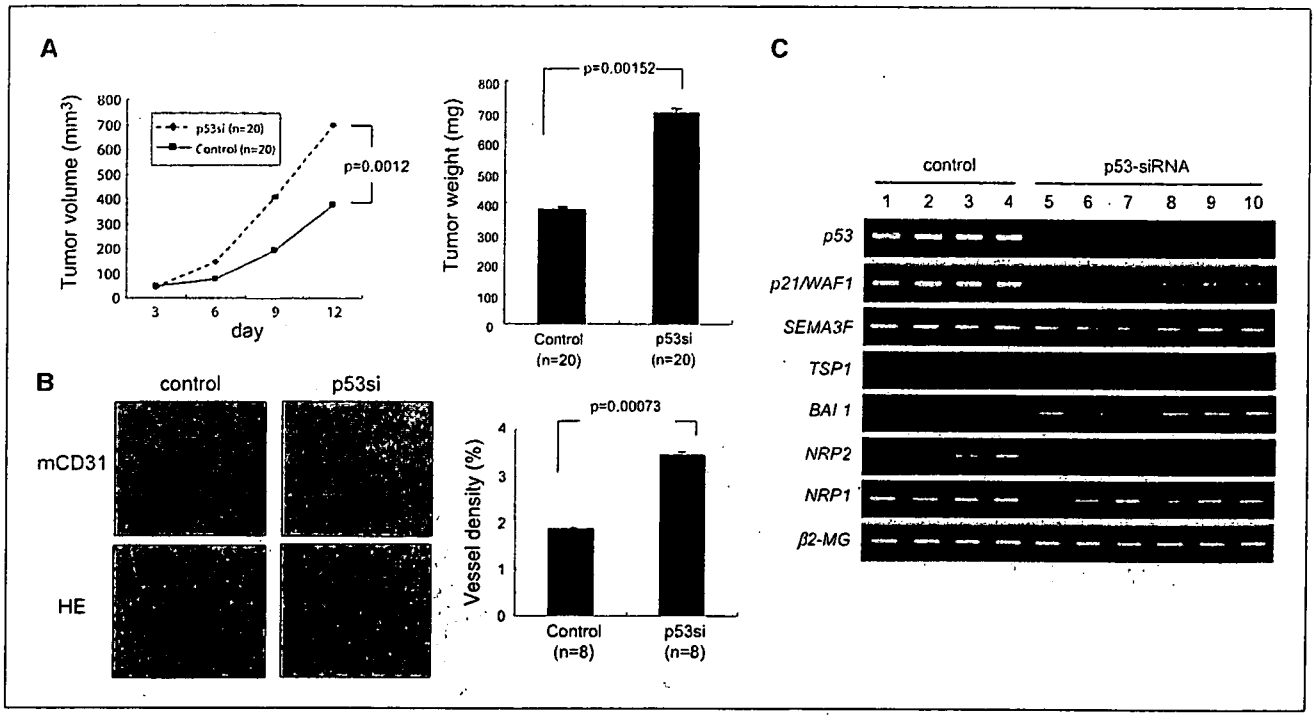

Figure 4. p53-regulated inhibition of tumor angiogenesis. *A*, involvement of p53 in suppression of tumor growth. *Left*, tumor volume. The tumor volume of each tumor derived from LS174T-p53-control (*control*) or LS174T-p53-siRNA (*p53si*) cell line was measured twice every week following the establishment of xenografts in BALB/c AJcl-nu nude mice. *Right, columns*, average tumor weight for each group; *bars*, SE. $P < 0.01$ was deemed statistically significant. *B*, p53-dependent suppression of tumor vessel formation. *Left*, immunohistochemistry for CD31 expression. Frozen sections of the isolated tumors from LS174T-p53-control or LS174T-p53-siRNA cell line were subjected to immunohistochemical staining with anti-CD31 antibody and H&E staining. Representative result from each group (×200). *Right*, measurement of the area of tumor blood vessels. The area of tumor blood vessels stained with anti-CD31 antibody was measured in the intratumoral region. *Columns*, average area of tumor vessels for each group; *bars*, SE. $P < 0.01$ was deemed statistically significant. *C*, expression levels of *p53, p21/WAF1, SEMA3F, TSP1, BAI1, NRP2*, and *NRP1* in each tumor were examined by RT-PCR. mRNAs were isolated from four LS174T-p53-control tumors (*1–4*) and six LS174T-p53-siRNA tumors (*5–10*) and were subjected to RT-PCR analysis. *β2-MG* was used as a quantitative control.

to form tumors. As shown in Fig. 4*A*, tumors derived from LS174T-p53-siRNA cells attained a volume of ~700 mm^3 by day 11 after inoculation, which is two times greater than the tumors from LS174T-control cells. Interestingly, it is absolutely evident that the number and area of tumor vessels in p53-knockdown tumors are much more and greater than those of tumor vessels in control tumors containing normal levels of p53 (Fig. 4*B* and Supplementary Fig. S3). The results clearly show that p53 is definitely involved in the suppression of tumor vessel formation.

To evaluate the role of antiangiogenic p53 target genes, including *TSP1, BAI1*, and *SEMA3F*, in this phenomenon, we examined the expression levels of these genes and several related genes in the tumors isolated at day 11. Interestingly, although the cells and tumors were not exposed to any genotoxic stress, the expression of *p53* mRNA was significantly elevated in the control tumors containing wild-type p53 but not in the p53-siRNA tumors (Fig. 4*C*). Consistent with the expression level of p53, *p21/WAF1* mRNA levels in the control tumors were higher than those in the p53-siRNA tumors. The expression levels of *SEMA3F* in control tumors seemed to be slightly but not remarkably higher than those in p53-knockdown tumors (Fig. 4*C*). On the other hand, the expression of *TSP1* was not detected in either tumors, and *BAI1* expression levels in control tumors were lower as compared with those in p53-knockdown tumors (Fig. 4*C*). Surprisingly, the expression of *NRP2*, the functional receptor for SEMA3F, was clearly elevated in control tumors as compared with p53-knockdown tumor (Fig. 4*C*).

To validate the role of SEMA3F in p53-regulated anti-angiogenesis of tumors, we expressed exogenous SEMA3F in p53-knockdown tumors. As shown in Supplementary Fig. S4, p53-knockdown tumors infected with Ad-SEMA3F revealed significant reductions in tumor size and tumor vessel density. Thus, these results support the notion that SEMA3F plays an important role in p53-regulated angiogenesis suppression.

Identification of NRP2 as a direct transcriptional target of p53. Because the expression levels of *NRP2* mRNA were severely impaired in p53-knockdown tumors (Fig. 4*C*), we speculated that NRP2 expression might be directly regulated by p53. To examine whether NRP2 is a direct transcriptional target of p53, we did several experiments (Fig. 5). As shown in Fig. 5*A*, the expression of *NRP2* mRNA was induced in response to DNA damage in a p53-dependent manner. Furthermore, we have found a p53-binding sequence (BS1) in promoter of the *NRP2* gene (Fig. 5*B*), and the sequence of BS1 interacted with p53 in the cells infected with Ad-p53 (Fig. 5*C*). Moreover, the sequence of BS1, but not BS2 (a negative control), actually had p53-dependent transcriptional activity in reporter assay (Fig. 5*D*). Interestingly, p63γ also activated to some extent the transcription of the luciferase-containing BS1 (Fig. 5*E*). These results suggest that *NRP2* is a direct target gene of p53 and that p63γ may be involved in the regulation of NRP2 expression.

The role of the SEMA3F-NRP2 signaling pathway in cell growth suppression. Based on the results of Figs. 1, 2, and 5, it is likely that p53 is directly involved in the transcription of both the

ligand SEMA3F and the receptor NRP2. Therefore, we assumed that the SEMA3F-NRP2 signaling pathway may play a role in cell growth control *in vitro*. To validate this assumption, we established the stable H1299 clone expressing NRP2 and prepared the adenovirus vector designed to express SEMA3F (Ad-SEMA3F) or FLAG-SEMA3F (Ad-FLAG-SEMA3F). As shown in Fig. 6*A*, the stable H1299 clone (s-11) highly expressed NRP2 whereas parental H1299 cells displayed low level of NRP2. Moreover, s-11 cells infected with Ad-SEMA3F or Ad-FLAG-SEMA3F revealed significant levels of *SEMA3F* mRNA or protein, respectively, in a dose-dependent manner (Fig. 6*B*).

By using these materials, we examined the effect of SEMA3F and NRP2 on *in vitro* cell growth rate. As expected, overexpression of EGFP did not induce any remarkable change of the cell growth rate of either parental or s-11 cells (Fig. 6*C*). However, the cells infected with Ad-SEMA3F or Ad-FLAG-SEMA3F clearly showed cell growth suppression in a dose-dependent manner (Fig. 6*C*). In addition, consistent with the result of Supplementary Fig. S1, overexpression of SEMA3F induced a maximum of 50% to 80% reduction in cell number in parental cells, whereas cell number in the s-11 clone infected with Ad-SEMA3F or Ad-FLAG-SEMA3F decreased to <10% of the control cells (without infection of Ad-SEMA3F or Ad-FLAG-SEMA3F; Fig. 6*C*). These results suggest that the SEMA3F-NRP2 signaling pathway may play a significant role in cell growth suppression as well as inhibition of tumor angiogenesis (Fig. 6*D*).

Discussion

Although *SEMA3F* was initially identified as a candidate tumor suppressor gene at chromosome 3p21.3, the causative point mutations in the *SEMA3F* gene are very rare in human cancers (17–19). This casts a doubt on the role of *SEMA3F* as a tumor suppressor gene. However, accumulating evidence continues to support the potential role of SEMA3F in tumorigenesis. For example, overexpression of SEMA3F in the mouse fibrosarcoma and human ovarian adenocarcinoma cell lines caused tumor growth suppression (23). This effect was confirmed by two studies. In the first study, ectopic expression of SEMA3F in the human embryonic kidney 293 cell line inhibited tumor formation in nude

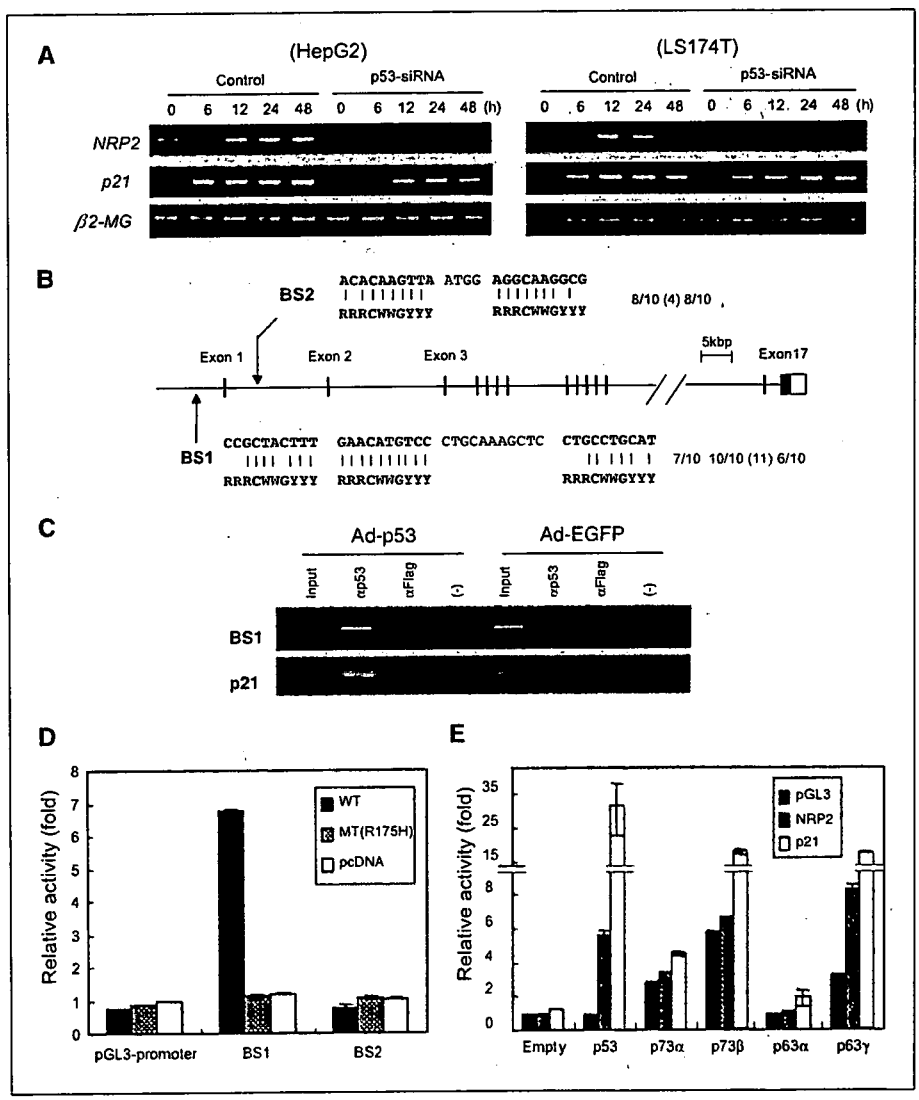

Figure 5. Identification of *NRP2* as a direct target gene of p53. *A*, endogenous p53–dependent expression of *NRP2*. RT-PCR analysis was done using mRNAs isolated at the indicated times from p53-siRNA and control cells (HepG2 or LS174T) as shown similarly in Fig. 1. *β2-MG* was used as an internal control. *B*, potential p53-binding sequences. Two potential p53-binding sequences, BS1 and BS2, are located at 3.5 kbp upstream of transcription starting site and in intron 1 of *NRP2* genome. *C*, binding of p53 with BS1 of *NRP2*. Chromatin immunoprecipitation assay was carried out for the DNA-protein complex, which was immunoprecipitated with anti-p53 antibody from HepG2 cells infected with either Ad-p53 or Ad-EGFP at an MOI of 30. *p21/WAF1* was used as a positive control. *D*, p53-dependent transcriptional activity of BS1. The heterologous luciferase reporter plasmid containing BS1 or BS2 for NRP2 was cotransfected with the plasmid designed to express wild-type p53 (p53WT), mutant p53 (p53MT), or no p53 (mock) into H1299 cells. The luciferase activity 24 h after transfection is shown in relation to the activity of the pGL3-promoter vectors without p53BSs. *E*, transcriptional activity of BS1 by p53-related genes. The heterologous luciferase reporter plasmid containing BS1 was cotransfected with the plasmid designed to express wild-type p53 (*p53*), p73α p73β, p63α, p63γ, or no p53 (mock) into H1299 cells. The luciferase activity 24 h after transfection is shown in relation to the activity of the pGL3-promoter vectors without p53BSs.

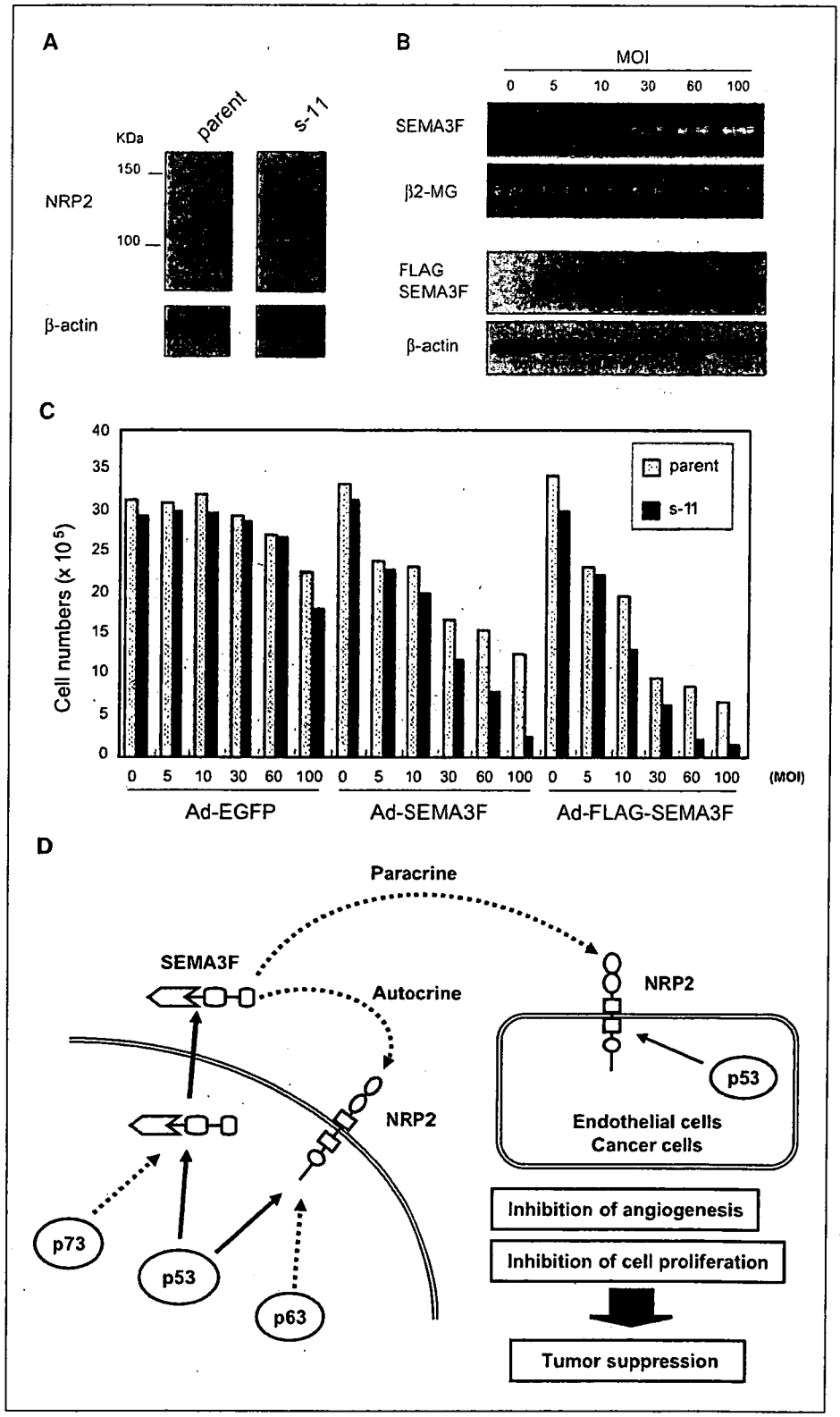

Figure 6. Involvement of the SEMA3F-NRP2 pathway in cell growth suppression. *A*, establishment of the H1299 stable transformant expressing NRP2. The expression of NRP2 in the parental and stable clone s-11 cell lines was shown by Western blotting. The expression of the NRP2 protein indicates two types of bands probably due to a protein modification. *B*, expression levels of SEMA3F mRNA and FLAG-SEMA3F protein. The s-11 cell line was infected with either Ad-SEMA3F or Ad-FLAG-SEMA3F at the indicated MOIs, and then the mRNAs and proteins were subjected to RT-PCR and Western blot analyses. *β2-MG* and *β-actin* were used as loading controls for RT-PCR and Western blotting, respectively. *C*, cell growth analysis. The cell numbers of either the parental or s-11 cell line were counted at 72 h after infection with Ad-EGFP, Ad-SEMA3F, or Ad-FLAG-SEMA3F at the indicated MOIs. *D*, hypothetical model for the p53-regulated SEMA3F-NRP2 tumor suppressive pathway.

mice and the resulting tumors displayed reduced density of tumor vessels, implying the role of SEMA3F in antiangiogenesis during tumor formation (39). The antiangiogenic activity of SEMA3F was also confirmed by both the *in vitro* cell growth inhibition assay for the human umbilical vein endothelial cells and the *in vivo* antiangiogenesis assay in this study (39). In the second study, the enforced expression of SEMA3F in highly metastatic human melanoma cells caused the phenotypic change from a highly

metastatic phenotype to a nonmetastatic and benign tumor-like phenotype, which is characterized by a large area of apoptosis, diminished vascularity, inhibition of hyperplasia in overlying epidermal cells, and encapsulated tumor borders delineated by thick layers of fibroblasts and collagen matrix (40). These observations suggest that SEMA3F definitely plays a role in preventing tumor progression through a common mechanism of antiangiogenesis. In the present study, we have also shown that overexpression of SEMA3F in a lung cancer cell line, H1299, caused a remarkable tumor growth suppression *in vivo*, and that this effect is likely to be mediated, at least in part, by the inhibition of tumor vessel formation. Therefore, consistent with the previous observations, we assume that SEMA3F indeed plays a role as a tumor suppressor gene by the down-regulation of tumor angiogenesis.

Thus far, two important mediators for antiangiogenesis, TSP1 and BAI1, were reported to be the transcriptional target genes of p53 (6, 7). In addition to these molecules, we have found that SEMA3F is the third antiangiogenic target gene. To determine whether TSP1, BAI1, and SEMA3F play some role in p53-regulated antiangiogenesis, we examined the expression levels of these genes in control LS174T tumors and p53-knockdown LS174T tumors. As shown in Fig. 4*C*, TSP1 expression was not detected in either control or p53-knockdown tumors, and BAI1 levels in control tumors were lower than those in p53-knockdown tumors. Therefore, TSP1 and BAI1 were unlikely to be involved in p53-regulated antiangiogenesis in our system that used the colorectal cancer cell line LS174T. On the other hand, control LS174T tumors displayed slightly higher expression levels of SEMA3F as compared with p53-knockdown tumors. These results suggest that, at least in our system that used LS174T colorectal cancer, SEMA3F may play some role in tumor angiogenesis suppression and that SEMA3F represents a new mediator for p53-regulated antiangiogenesis.

The surprising finding is that the expression of NRP2, the functional receptor for SEMA3F, depended on the status of p53 in the tumors (Fig. 4*C*). Indeed, we have found that the *NRP2* gene has a p53-responsive and binding sequence and that the expression of NRP2 is inducible in response to exogenous and endogenous p53, implying that NRP2 is also a p53 target gene (Fig. 5). This observation gives rise to several hypotheses. First, p53 may regulate both SEMA3F and its receptor NRP2, thereby the p53-activated SEMA3F is secreted and binds to NRP2 present on the cell secreting SEMA3F, leading to cell growth suppression in an autocrine fashion. Second, the secreted SEMA3F binds to NRP2 on vascular endothelial cells that express NRP2 on their surface, leading to inhibition of tumor vessel formation in a paracrine fashion. Third, the secreted SEMA3F binds to NRP2 on the surface of neighboring tumor cells, leading to growth suppression of tumor cells. Fourth, p53 may function as a bystander to express and secrete SEMA3F, which binds to NRP2 on the surface of the target cancer cell and induces growth suppression of the target cells. Fifth, again p53 may function as a bystander to express NRP2 on the surface of vascular endothelial cells that bind to the tumor-secreted SEMA3F, leading to antiangiogenesis under the control of p53. Several other hypotheses may arise as a result of further studies. Consistent with these assumptions, the SEMA-NRP2 pathway, in fact, controlled not only tumor angiogenesis but also the *in vitro* cell growth of cancer cells (Fig. 6*C*). In any case, p53 would regulate both cell growth itself and tumor angiogenesis in an autocrine or paracrine fashion (Fig. 6*D*). The role of p53 as a bystander in the surrounding cells including cancer cells, endothelial cells, fibroblast cells, immune cells, etc., would be considerably important for the prevention of tumor progression via the SEMA3F-NRP2 pathway.

In our *in vivo* assay, SEMA3F revealed a more remarkable inhibitory effect on tumor growth compared with the *in vitro* assay. According to the *in vitro* result on the same H1299 cells (Supplementary Figs. S1 and S2), the effect was likely mediated by the communication between the secreted SEMA3F protein and its receptor NRP2 expressed in the surrounding cells, including epithelial cells and fibroblasts. Consistent with this notion, the parental H1299 cells do not express high levels of NRP2 protein (Fig. 6*A*). Because we used the human SEMA3F protein in the mouse system, this will raise one important question about whether human SEMA3F can interact with mouse NRP2 receptor. However, the sequence homology reveals >96% identity between human and mouse SEMA3F protein. In addition, it shows >94% identity between human and mouse NRP2 protein. Based on the very high homology of SEMA3F or NRP2 between human and mouse, we assume that human SEMA3F probably interacts with mouse NRP2 in our assay. Thus, we think that the results in the *in vivo* assay support the paracrine model for the SEMA3F-NRP2 pathway (Fig. 6*D*).

In contrast to SEMA3B, which is the neighboring SEMA member at 3p21.3 and whose function is involved in apoptosis (33, 41), many lung cancers continue to express SEMA3F in spite of p53 mutations (18). This seems to be the long-lasting issue for the role of SEMA3F in the 3p21.3 tumor suppressor genes. However, our two findings provide some clue to address this question. First, the expression of SEMA3F is likely regulated not only by p53 but also by p73, the function of which is usually normal in human lung cancers. This implies that inactivation of p53 does not necessarily lead to the total down-regulation of SEMA3F expression. Second, it seems that the expression of NRP2 is very critical for the SEMA3F-NRP2 autocrine pathway (Fig. 6*D*). In our data, the expression of NRP2 was more dependent on p53 in the tumors (Fig. 4*C*) and NRP2 was also a direct target gene of p53 (Fig. 5). Therefore, not SEMA3F but NRP2 might be the key target for lung cancer tumorigenesis via the p53-SEMA3F-NRP2 pathway. To clarify the precise regulatory mechanism for the SEMA3F-NRP2 pathway, further investigation is needed for the role of NRP2 in human primary lung cancers.

How does SEMA3F suppress tumor progression and metastasis? The precise mechanism for the SEMA3F-dependent pathway still remains largely unclear. However, SEMA3F may be involved in the regulation of angiogenesis and metastasis. In SEMA3F-regulated antiangiogenesis, the target cell that expresses NRP2 is likely to play a critical role in the antiangiogenic activity. Thus far, the expression of NRP2 has been found in vascular endothelial cells (42), lymphatic endothelial cells (43), and possibly cancer cells. Therefore, vascular endothelial cells or lymphatic endothelial cells may be SEMA3F target cells. However, recent observations have provided evidence that the recruitment of bone marrow–derived endothelial precursor cells contributes to tumor vasculature (44–46). Although it is still unclear whether bone marrow–derived endothelial precursor cells express the SEMA3F receptor(s), including NRP2, it will be interesting to investigate whether SEMA3F suppresses the recruitment of bone marrow–derived endothelial precursor cells to the site of tumor vessel formation. Moreover, in cancer metastasis, the previous reports clearly showed that SEMA3F prevents *in vivo* tumor metastasis (35, 40) and that SEMA3F inhibits *in vitro* cell

attachment and motility (47, 48). Very recently, a study reported that the premetastatic niche initiated by vascular endothelial growth factor receptor 1–positive hematopoietic bone marrow progenitor cells (VHBMPC) is very critical for the establishment of cancer metastasis at the metastatic site (49). We speculate that SEMA3F might prevent cancer metastasis by inhibiting the recruitment of VHBMPCs at the premetastatic niche. Therefore, it is also interesting to investigate whether VHBMPCs express the functional SEMA3F receptor(s) and whether SEMA3F actually inhibits cell attachment, motility, and proliferation of VHBMPCs.

We believe that further investigation on the SEMA3F-NRP2 pathway will clarify the mechanism for the p53-regulated communication between cancer cells and the surrounding cells and the mechanism for the SEMA3F-regulated pathways of antiangiogenesis and antimetastasis. In addition, application of the SEMA3F pathway will definitely initiate the development of novel strategies for cancer therapy.

Acknowledgments

Received 7/7/2006; revised 10/31/2006; accepted 12/6/2006.

Grant support: Ministry of Health, Labor, and Welfare, Japan, and the Ministry of Education, Culture, Sports, Science, and Technology, Japan.

The costs of publication of this article were defrayed in part by the payment of page charges. This article must therefore be hereby marked *advertisement* in accordance with 18 U.S.C. Section 1734 solely to indicate this fact.

We thank B. Vogelstein for the p53-knockout colorectal cancer cell lines; S. Ikawa for the plasmids for p73α, p73β, p63α, and p63γ; T. Kiyono for the retrovirus vector for p53-siRNA; and S. Usuda, A. Ishizaka, and I. Ryo for their technical assistance.

References

1. Vogelstein B, Lane D, Levine AJ. Surfing the p53 network. Nature 2000;408:307–10.
2. Vousden KH. Live or let die: The cell's response to p53. Nat Rev Cancer 2002;2:594–604.
3. Nakamura Y. Isolation of p53-target genes and their functional analysis. Cancer Sci 2004;95:7–11.
4. Arakawa H. p53, apoptosis and axon-guidance molecules. Cell Death Differ 2005;12:1057–65.
5. Van Meir EG, Polverini PJ, Chazin VR, Su Huang HJ, de Tribolet N, Cavenee WK. Release of an inhibitor of angiogenesis upon induction of wild type p53 expression in glioblastoma cells. Nat Genet 1994;8:171–6.
6. Dameron KM, Volpert OV, Tainsky MA, Bouck N. Control of angiogenesis in fibroblasts by p53 regulation of thrombospondin-1. Science 1994;265:1582–4.
7. Nishimori H, Shiratsuchi T, Urano T, et al. A novel brain-specific p53-target gene, BAI1, containing thrombospondin type 1 repeats inhibits experimental angiogenesis. Oncogene 1997;15:2145–50.
8. Nakamura F, Kalb RG, Strittmatter SM. Molecular basis of semaphorin-mediated axon guidance. J Neurobiol 2000;44:219–29.
9. Tamagnone L, Comoglio PM. Signalling by semaphorin receptors: cell guidance and beyond. Trends Cell Biol 2000;10:377–83.
10. Tamagnone L, Comoglio PM. To move or not to move? Semaphorin signalling in cell migration. EMBO Rep 2004;5:356–61.
11. Yu TW, Bargmann CI. Dynamic regulation of axon guidance. Nat Neurosci 2001;4 Suppl:1169–76.
12. Semaphorin Nomenclature Committee. Unified nomenclature for the semaphorins/collapsins. Cell 1999;97:551–2.
13. Chen H, Chedotal A, He Z, Goodman CS, Tessier-Lavigne M. Neuropilin-2, a novel member of the neuropilin family, is a high affinity receptor for the semaphorines Sema E and Sema IV but not Sema III. Neuron 1997;19:547–59.
14. Chen H, He Z, Bagri A, Tessier-Lavigne M. Semaphorin-neuropilin interactions underlying sympathetic axon responses to class III semaphorins. Neuron 1998;21:1283–90.
15. Chen H, Bagri A, Zupicich JA, et al. Neuropilin-2 regulates the development of selective cranial and sensory nerves and hippocampal mossy fiber projections. Neuron 2000;25:43–56.
16. Sahay A, Molliver ME, Ginty DD, Kolodkin AL. Semaphorin 3F is critical for development of limbic system circuitry and is required in neurons for selective CNS axon guidance events. J Neurosci 2003;23:6671–80.
17. Xiang RH, Hensel CH, Gracia DK, et al. Isolation of the human semaphoring III/F gene (SEMA3F) at chromosome 3p21, a region deleted in lung cancer. Genomics 1996;32:39–48.
18. Sekido Y, Bader S, Latif F, et al. Human semaphorins A(V) and IV reside in the 3p21.3 small lung cancer deletion region and demonstrate distinct expression patterns. Proc Natl Acad Sci U S A 1996;93:4120–5.
19. Roche J, Bold F, Robinson M, et al. Distinct 3p21.3 deletions in lung cancer and identification of a new human semaphorin. Oncogene 1996;12:1289–97.
20. Brauch H, Johnson B, Hovis J, et al. Molecular analysis of the short arm of chromosome 3 in small-cell and non-small-cell carcinoma of the lung. N Engl J Med 1987;317:1109–13.
21. Kok K, Osinga J, Carritt B, et al. Deletion of a DNA sequence at the chromosomal region 3p21 in all major types of lung cancer. Nature 1987;330:578–81.
22. Kusy S, Potiron V, Zeng C, et al. Promoter characterization of Semaphorin SEMA3F, a tumor suppressor gene. Biochim Biophys Acta 2005;1730:66–76.
23. Xiang R, Davalos AR, Hensel CH, Zhou XJ, Tse C, Naylor SL. Semaphorin 3F gene from human 3p21.3 suppresses tumor formation in nude mice. Cancer Res 2002;62:2637–43.
24. Hara S, Nakashima S, Kiyono T, et al. p53-independent ceramide formation in human glioma cells during γ-radiation-induced apoptosis. Cell Death Differ 2004;11:53–61.
25. Nakamura Y, Futamura M, Kamino H, et al. Identification of p53-46F as a super p53 with an enhanced ability to induce p53-dependent apoptosis. Cancer Sci 2006;97:633–41.
26. Masuda Y, Futamura M, Kamino H, et al. The potential role of DFNA5, a hearing impairment gene, in p53-mediated cellular response to DNA damage. J Hum Genet 2006;51:645–51.
27. Ishimoto O, Kawahara C, Enjo K, Obinata M, Nukiwa T, Ikawa S. Possible oncogenic potential of ΔNp73: a newly identified isoform of human p73. Cancer Res 2002;62:636–41.
28. Osada M, Ohba M, Kawahara C, et al. Cloning and functional analysis of human p51, which structurally and functionally resembles p53. Nat Med 1998;4:839–43.
29. Oda K, Arakawa H, Tanaka T, et al. p53AIP1, a potential mediator of p53-dependent apoptosis, and its regulation by Ser-46-phosphorylated p53. Cell 2000;102:849–62.
30. Prewett M, Huber J, Li Y, et al. Antivascular endothelial growth factor receptor (fetal liver kinase 1) monoclonal antibody inhibits tumor angiogenesis and growth of several mouse and human tumors. Cancer Res 1999;59:5209–18.
31. Tang T, Nakada MT, Kasavan P, et al. Extracellular matrix metalloproteinase inducer stimulates tumor angiogenesis by evaluating vascular endothelial cell growth factor and matrix metalloproteinase. Cancer Res 2005;65:3193–9.
32. Arakawa H. Netrin-1 and its receptors in tumorigenesis. Nat Rev Cancer 2004;4:978–87.
33. Ochi K, Mori T, Toyama Y, Nakamura Y, Arakawa H. Identification of semaphorin3B as a direct target of p53. Neoplasia 2002;4:82–7.
34. Serini G, Valdembri D, Zanivan S, et al. Class 3 semaphorins control vascular morphogenesis by inhibition intergrin function. Nature 2003;424:391–7.
35. Bielenberg DR, Pettaway CA, Takashima S, Klagsbrun M. Neuropilins in neoplasms: expression, regulation, and function. Exp Cell Res 2006;312:584–93.
36. Eichmann A, Makinen T, Alitalo K. Neural guidance molecules regulate vascular remodeling and vessel navigation. Genes Dev 2005;19:1013–21.
37. Suchting S, Bicknell R, Eichmann A. Neural clues to vascular guidance. Exp Cell Res 2006;312:668–75.
38. Potiron V, Roche J. Class 3 semaphorin signaling: the end of a dogma. Sci STKE 2005;285:pe24.
39. Kessler O, Shraga-Heled N, Lange T, et al. Semaphorin-3F is an inhibitor of tumor angiogenesis. Cancer Res 2004;64:1008–15.
40. Bielenberg DR, Hida Y, Shimizu A, et al. Semaphorin 3F, a chemorepulsant for endothelial cells, induces a poorly vascularized, encapsulated, nonmetastatic tumor phenotype. J Clin Invest 2004;114:1260–71.
41. Castro-Rivera E, Ran S, Thorpe P, Minna JD. Semaphorin 3B (SEMA3B) induces apoptosis in lung and breast cancer, whereas VEGF165 antagonizes this effect. Proc Natl Acad Sci U S A 2004;101:11432–7.
42. Herzog Y, Kalcheim C, Kahane N, Reshef R, Neufeld G. Differential expression of neuropilin-1 and neuropilin-2 in arteries and veins. Mech Dev 2001;109:115–9.
43. Yuan L, Moyon D, Pardanaud L, et al. Abnormal lymphatic vessel development in neuropilin 2 mutant mice. Development 2002;129:4797–806.
44. Lyden D, Hattori K, Dias S, et al. Impaired recruitment of bone-marrow-derived endothelial and hematopoietic precursor cells blocks tumor angiogenesis and growth. Nat Med 2001;7:1194–201.
45. Peters BA, Diaz LA, Polyak K, et al. Contribution of bone marrow-derived endothelial cells to human tumor vasculature. Nat Med 2005;11:261–2.
46. Garmy-Susini B, Varner JA. Circulating endothelial progenitor cells. Br J Cancer 2005;93:855–8.
47. Nasarre P, Constantin B, Rouhaud L, et al. Semaphorin SEMA3F and VEGF have opposing effects on cell attachment and spreading. Neoplasia 2003;5:83–92.
48. Nasarre P, Kusy S, Constantin B, et al. Semaphorin SEMA3F has a repulsing activity on breast cancer cells and inhibits E-cadherin-mediated cell adhesion. Neoplasia 2005;7:180–9.
49. Kaplan RN, Riba RD, Zacharoulis S, et al. VEGFR1-positive hematopoietic bone marrow progenitors initiate the pre-metastatic niche. Nature 2005;438:820–7.

nature genetics

Mutation of *RRM2B*, encoding p53-controlled ribonucleotide reductase (p53R2), causes severe mitochondrial DNA depletion

Alice Bourdon[1], Limor Minai[1], Valérie Serre[1,2], Jean-Philippe Jais[3], Emmanuelle Sarzi[1], Sophie Aubert[1], Dominique Chrétien[1], Pascale de Lonlay[1], Véronique Paquis-Flucklinger[4], Hirofumi Arakawa[5], Yusuke Nakamura[5], Arnold Munnich[1] & Agnès Rötig[1]

Mitochondrial DNA (mtDNA) depletion syndrome (MDS; MIM 251880) is a prevalent cause of oxidative phosphorylation disorders characterized by a reduction in mtDNA copy number. The hitherto recognized disease mechanisms alter either mtDNA replication (*POLG* (ref. 1)) or the salvage pathway of mitochondrial deoxyribonucleosides 5′-triphosphates (dNTPs) for mtDNA synthesis (*DGUOK* (ref. 2), *TK2* (ref. 3) and *SUCLA2* (ref. 4)). A last gene, *MPV17* (ref. 5), has no known function. Yet the majority of cases remain unexplained. Studying seven cases of profound mtDNA depletion (1–2% residual mtDNA in muscle) in four unrelated families, we have found nonsense, missense and splice-site mutations and in-frame deletions of the *RRM2B* gene, encoding the cytosolic p53-inducible ribonucleotide reductase small subunit. Accordingly, severe mtDNA depletion was found in various tissues of the *Rrm2b*$^{-/-}$ mouse. The mtDNA depletion triggered by p53R2 alterations in both human and mouse implies that p53R2 has a crucial role in dNTP supply for mtDNA synthesis.

A genome-wide linkage analysis using Affymetrix gene-chip SNP array in a large inbred Moroccan family (**Fig. 1**) with severe muscle mtDNA depletion (1% of control, **Fig. 2**) showed a single region of autozygosity on chromosome 8q21.3–q22.3 (log likelihood ratio (lod) score 3.331). This 12.1-Mb region encompasses 60 genes. We sequenced and excluded five genes encoding known or putative mitochondrial proteins (*UQCRB*, *MTERFD1*, *HRSP12*, *COX6C* and *SLC25A32*) and three genes encoding proteins involved in either phospholipid biosynthesis (*PTDSS1*) or RNA metabolism (*RBM12B* and *POP1*).

Based on its critical function in nucleotide synthesis, the *RRM2B* gene, encoding the ribonucleotide reductase small subunit inducible by the tumor suppressor p53, was selected for further analysis. Ribonucleotide reductase is a heterotetrameric enzyme responsible for *de novo* conversion of ribonucleoside 5′-diphosphates into deoxyribonucleoside 5′-diphosphates, essential for DNA synthesis[6]. This enzyme, which consists of one homodimeric R1 subunit and one homodimeric R2 subunit, is in charge of dNTPs synthesis during the S phase of the cell cycle. Recently p53R2 has been identified as a p53-induced R2 homolog, allowing dNTP supply for DNA repair[7].

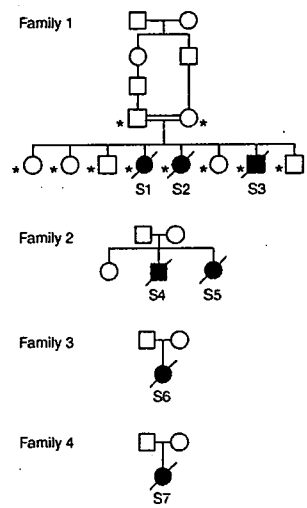

Figure 1 Pedigrees. Filled symbols indicate affected individuals; symbols with slashes indicate deceased. Asterisks in family 1 indicate individuals enrolled in the genome-wide linkage analysis.

[1]Institut national de la santé et de la recherche médicale U781 and Service de Génétique, Hôpital Necker-Enfants Malades, 149 rue de Sèvres, 75015 Paris, France. [2]Université Paris 7, 2 Place Jussieu, 75005 Paris, France. [3]Service de biostatistique et Informatique Médicale Université René Descartes, Faculté de Médecine, Hôpital Necker-Enfants Malades, 149 rue de Sèvres, 75015 Paris, France. [4]Department of Medical Genetics, Archet 2 Hospital, 151 Route St Antoine de Ginestière, 06107 Nice, France. [5]Human Genome Center, Institute of Medical Science, University of Tokyo, 4-6-1 Shirikanedai, Minato-ku, Tokyo 108-8639, Japan. Correspondence should be addressed to A.R. (roetig@necker.fr).

Received 23 January; accepted 10 April; published online 7 May 2007; doi:10.1038/ng2040

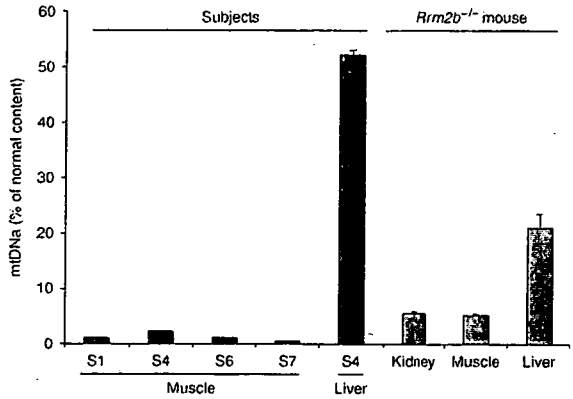

Figure 2 Real-time PCR quantification of the mtDNA content relative to that of *MLH1* or *Pde6b* nuclear genes used as references for human or mouse respectively. The measurements were repeated three times. $P < 0.0001$ for all patient tissues and mouse liver and <0.001 for mouse kidney and muscle. Error bars, s.d.

Sequencing exons and flanking intronic regions of the gene detected an nt 850 C>T homozygous mutation in all affected individuals, whereas parents were heterozygous for this mutation (which results in a Q284X substitution, in which Gln284 is replaced by a stop codon; **Supplementary Fig. 1** online). Sequencing the *RRM2B* gene in four additional individuals with severe muscle mtDNA depletion (to 1–2% of control mtDNA amount; **Fig. 2**) in three other families identified additional deleterious mutations (**Supplementary Fig. 1**). The two affected sibs in family 2 (subjects 4 and 5) were compound heterozygotes for a splice-site mutation (IVS3-2 A>G inherited from the mother) and a missense mutation (nt 580 G>A inherited from the father, E194K; **Supplementary Fig. 1**). The missense mutation identified in subjects 4 and 5 appeared to be homozygous at the cDNA level (**Supplementary Fig. 1**), implying that the splice-site mutation (IVS3-2 A>G) caused an mRNA decay. The proband in family 3 (subject 6) was also compound heterozygote for two missense mutations (nt 190 T>C, W64R, and nt 581 A>G, E194G; **Supplementary Fig. 1**). Finally, the proband in family 4 (subject 7) harbored a 3-bp in-frame deletion (nt 253–255 ΔGAG, ΔGlu85) and a missense mutation (nt 707 G>T, C236F; **Supplementary Fig. 1**). The missense mutations and the 3-bp deletion affected amino acid residues that are highly conserved across species in all small ribonucleotide reductase protein subunits (**Supplementary Fig. 2** online). We found none of these mutations in more than 220 control chromosomes from the same ethnic origin, nor in any human EST. Finally, we did not identify any *RRM2B* mutations in seven individuals with less severe muscle mtDNA depletion (10–30% of normal mtDNA amount).

Rrm2b$^{-/-}$ mice show growth retardation, renal failure, muscle atrophy and early mortality[8], consistent with a mitochondrial disorder despite the absence of overt respiratory chain deficiency (not shown). *Rrm2b*$^{-/-}$ mice at 12 weeks of age had a markedly decreased mtDNA content, as measured by quantitative real-time PCR in kidney, muscle and liver (respectively 5.57% ± 0.26%, $P < 0.01$; 5.24% ± 0.21%, $P < 0.01$; and 21.04% ± 2.46, $P < 0.001$, mean ± s.d. of age-matched control mtDNA amounts; **Fig. 2**).

The high degree of identity between R2 and p53R2 (83.5%) prompted us to model the structure of human p53R2 using the X-ray coordinates of the human R2 subunit as a tertiary template. As R2 and p53R2 structures are entirely α-helical, both N and C termini are unstructured and not visible (**Fig. 3**). p53R2 homodimeric docking, performed using the *ClusPro* web server software[9,10], showed that, as previously reported for *E. coli* R2 modeling[11], the p53R2 dimer is heart-shaped (**Fig. 3**). The crystal structure of the R1 subunit using a synthetic 20-residue peptide corresponding to the R2 C terminus of *E. coli*, as well as binding competition assays, have previously delineated the interaction between R1 and R2. Based on R1-R2 interaction in *E. coli*[11], **Figure 3** suggests the most likely interface of interaction between human R1 and p53R2 homodimers. The Q284X substitution in subjects 1–3 resulted in the deletion of the last 68 C-terminal residues, including part of an α-helix as well as the heptapeptide involved in the binding to R1 (ref. 12). Amino acid residue Glu194, which was mutated in families 2 (E194K) and 3 (E194G), is one of the three residues involved in iron binding, along with Glu228 and His231 (ref. 13; **Fig. 3** and **Supplementary Fig. 2**). The Trp64 residue mutated in family 3 (W64R) is one of the amino acids allowing the binding of R2 or p53R2 to the R1 subunit and the subsequent transfer of a tyrosyl radical needed for reduction of ribonucleotides[13]. Because Glu85 is predicted to form a hydrogen bond with Lys82, its deletion in subject 7 is expected to disrupt the local subdomain structure and the dimerization interface between R1 and R2 (**Fig. 3**). Finally, the Cys236 residue mutated in subject 7 is located near the iron binding sites and in a predicted ferritin-like domain of the protein (**Fig. 3**).

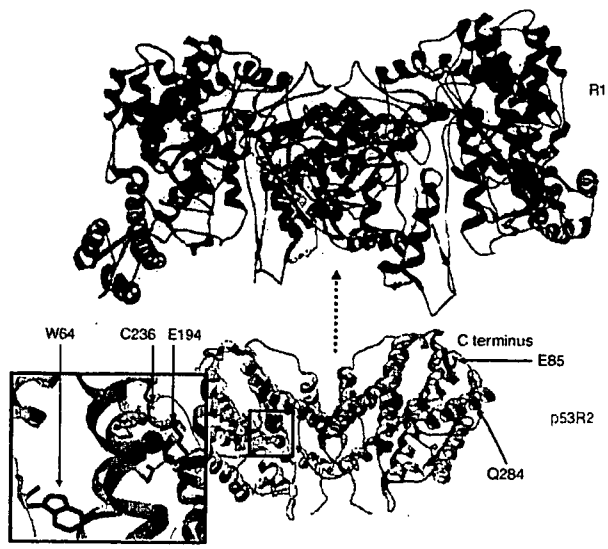

Figure 3 Computational modeling based on the crystal structure of the *E. coli* R1 and human R2 showing the putative R1-p53R2 interface of interaction. The crystal structure of *E. coli* R1 dimer (R1, dark blue and light blue) determined as a complex with the 20 residues of the carboxyl end of *E. coli* R2 (yellow) is shown. The R1 active sites are indicated in gray. The structure model of human p53R2 homodimeric docking is in yellow (R2). Residues of the carboxyl end of p53R2 (before L35) are labile and therefore not visible. The iron centers are shown as blue spheres. The Gln284 residue before the helix missing because of the Q284X substitution is indicated, as is the p53R2 C terminus. Inset: magnification of the second p53R2 iron-binding center. The Glu194 (red), Glu228 and His231 residues (pink) are the three involved in iron binding. Arrows indicate the residues altered in the mutants (Trp64 in green, Glu194 in red, Cys236 in light blue and Glu85 in green). The dotted arrow indicates the hypothetical interface of interaction between R1 and p53R2.